

# Designing Catalysts for Chirality-Selective Synthesis of Single-Walled Carbon Nanotubes: Past Success and Future Opportunity

Maoshuai He,\* Shuchen Zhang, Qianru Wu, Han Xue, Benwu Xin, Dan Wang, and Jin Zhang\*

A major obstacle for the applications of single-walled carbon nanotubes (SWNTs) in electronic devices is their structural diversity, ending in SWNTs with diverse electrical properties. Catalytic chemical vapor deposition has shown great promise in directly synthesizing high-quality SWNTs with a high selectivity to specific chirality ( $n, m$ ). During the growth process, the tube–catalyst interface plays crucial roles in regulating the SWNT nucleation thermodynamics and growth kinetics, ultimately governing the SWNT chirality distribution. Starting with the introduction of SWNT growth modes, this review seeks to extend the knowledge about chirality-selective synthesis by clarifying the energetically favored SWNT cap nucleation and the threshold step for SWNT growth, which describes how the tube–catalyst interface affects both the nucleus energy and the new carbon atom incorporation. Such understandings are subsequently applied to interpret the ( $n, m$ ) specific growth achieved on a variety of templates, such as SWNT segments or predefined molecular seeds, transition metal (Fe, Co and Ni)-containing catalysts at low reaction temperatures, W-based alloy catalysts, and metal carbides at relatively high reaction temperatures. The up to date achievements on chirality-controlled synthesis of SWNTs is summarized and the remaining major challenges existing in the SWNT synthesis field are discussed.

consist of 2–50 walls with diameters ranging from 5 to 20 nm. With the addition of metal catalysts into the cathodes, carbon nanotubes with single atomic-layer wall, named single-walled carbon nanotubes (SWNTs), were produced two years later.<sup>[2,3]</sup> SWNTs represent a novel class of low-dimensional materials exhibiting remarkable properties, predicated by theory<sup>[4,5]</sup> prior to their synthesis.

The exceptional fundamental electrical and structural properties of SWNTs arise from the strong carbon-carbon bond and the symmetric arrangement of carbon atoms.<sup>[6]</sup> SWNT is an analogue to monolayer graphene and can be visualized as a seamless cylinder rolled up from a layer of honeycomb-structured graphene (Figure 1a). As the width of parent graphene layer varies, the diameter of a structure-stable SWNT can range from 0.4 nm for the smallest SWNTs<sup>[7]</sup> to over 7 nm for SWNTs catalyzed by large-size particles.<sup>[8]</sup> Owing to the differences in rolling up direction, the chiral angle of SWNTs varies from 0° to 30°. The combination of diameter ( $d$ ) and chiral angle ( $\theta$ ) well defines the atomic structure of a SWNT, which can be alternatively assigned by a pair of chiral indices ( $n, m$ ) deduced from the chiral vector (Figure 1b). Most of SWNT properties depend sensitively on its chiral indices and such a dependence is non-monotonic.<sup>[9]</sup>

## 1. Introduction

The landmark work of Iijima in 1991 brought carbon nanotubes to the attention of the global scientific community.<sup>[1]</sup> The “microtubules of graphitic carbon” generated by arc-discharge


combination of diameter ( $d$ ) and chiral angle ( $\theta$ ) well defines the atomic structure of a SWNT, which can be alternatively assigned by a pair of chiral indices ( $n, m$ ) deduced from the chiral vector (Figure 1b). Most of SWNT properties depend sensitively on its chiral indices and such a dependence is non-monotonic.<sup>[9]</sup>

Prof. M. He, Prof. D. Wang  
Key Laboratory of Eco-Chemical Engineering  
Ministry of Education  
College of Chemistry and Molecular Engineering  
Qingdao University of Science and Technology  
Qingdao 266042, China  
E-mail: hemaoshuai@qust.edu.cn

Prof. M. He, Q. Wu, H. Xue, B. Xin  
School of Materials Science and Engineering  
Shandong University of Science and Technology  
Qingdao 266590, China

Dr. S. Zhang, Prof. J. Zhang  
Center for Nanochemistry  
Beijing Science and Engineering Center for Nanocarbons  
Beijing National Laboratory for Molecular Sciences (BNLMS)  
College of Chemistry and Molecular Engineering  
Peking University  
Beijing 100871, China  
E-mail: jinzhang@pku.edu.cn

Prof. D. Wang  
State Key Laboratory of Multi-Phase Complex Systems  
Institute of Process Engineering  
Chinese Academy of Sciences  
Beijing 100190, China

 The ORCID identification number(s) for the author(s) of this article can be found under <https://doi.org/10.1002/adma.201800805>.

DOI: 10.1002/adma.201800805

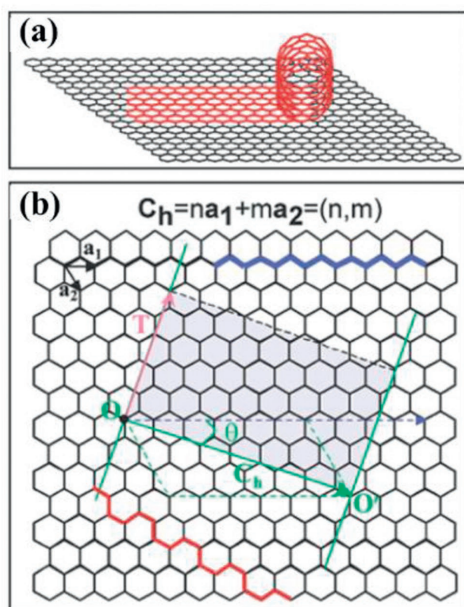


**Figure 1.** a) Schematic of the formation of an SWNT structure by rolling up a graphene sheet; b)  $OO'$  defines the chiral vector  $C_h = na_1 + ma_2 = (n, m)$ . Translation vector  $T$ , is perpendicular to  $C_h$ . The chiral angle  $\theta$  is defined as the angle between  $C_h$  and the  $(n, 0)$  zigzag direction. a, b) Reproduced with permission.<sup>[10]</sup> Copyright 2002, American Chemical Society.

A SWNT exhibits either metallic ( $n - m = 3i$ ) features with no apparent band gap or semiconducting ( $n - m = 3i \pm 1$ ) characteristics with a band gap inversely proportional to its diameter. The ability to directly yield both metallic and semiconducting SWNTs leads to the speculation that they can serve as key building blocks in carbon-based nanoelectronics.<sup>[10]</sup> Many game-changing electronic applications, have been conceived for SWNTs. For instance, in semiconductor industry where the miniaturization of electronic devices has been the principal driving force, SWNTs are likely candidates to replace silicon because of their lower electrical resistance and much less heat generated.<sup>[11,12]</sup> Indeed, a computer prototype whose central processor based entirely on SWNTs was released on 2013.<sup>[13]</sup> However, due to SWNT structure diversity, the SWNT computer processor is simple and slow. To reach the superb performance level of theoretically offered by SWNTs, it is necessary to develop ways to remove the material hurdle that prevents the creation of complex SWNT circuits.

From theoretical predications<sup>[4,14]</sup> and experimental characterizations,<sup>[15,16]</sup> most SWNT products consist of 1/3 metallic species and 2/3 semiconducting species. SWNTs with controlled structures and identical properties are required for many practical applications in nanoelectronics and optoelectronics. For example, a high-performance integrated circuit would involve of billions of identical semiconducting SWNT-based field-effect transistors with a metallic SWNT impurity of less than 0.0001%.<sup>[17]</sup> On the contrary, high-purity metallic SWNTs are desirable substitutes of ITO when applied in transparent conducting film.<sup>[18]</sup> Consequently, the foreseeable future of SWNTs is heavily reliant on the property uniformity of the supplied SWNTs.<sup>[19]</sup> Several post-growth techniques, including density gradient ultracentrifugation,<sup>[20]</sup> DNA recognition<sup>[21]</sup> and gel chromatography,<sup>[22]</sup> have been



**Maoshuai He** received his Ph.D. degree in chemistry from Peking University in 2006. After working as a postdoctoral fellow in Centre National de la Recherche Scientifique (CNRS) in France and Aalto University in Finland, he joined Shandong University of Science and Technology in 2016. In 2018, he moved to Qingdao

University of Science and Technology. His research is focused on controlled synthesis and applications of carbon nanomaterials.



**Jin Zhang** received his Ph.D. degree from Lanzhou University in 1997. After a 2-year postdoctoral fellowship at the University of Leeds, UK, he returned to Peking University where he was appointed as an associate professor in 2000 and promoted to a full professor in 2006. In 2013, he was appointed as Changjiang

professor. His research focuses on the controlled synthesis and spectroscopic characterization of carbon nanomaterials.

developed for sorting SWNTs according to their conductivities or chiralities.<sup>[23,24]</sup> However, these approaches usually suffer high cost and are rather complicated.<sup>[23]</sup> More importantly, the sorting process would inevitably destroy the perfect structures of SWNTs and deteriorate their pristine properties. Consequently, directly synthesizing SWNTs with single chirality is regarded as a cost-effective approach to meet the SWNT market demands.

Arc-discharge method is initially applied for generating SWNTs.<sup>[2,3]</sup> Subsequently, a laser ablation technique is developed to evaporate transition metal/graphite composite rods in inert gas for creating SWNTs.<sup>[25]</sup> The high processing temperatures (above 1700 °C for arc discharge and  $\approx 1200$  °C for laser ablation) and the lack of control over SWNT growth in gas phase inhibit their wide applications for SWNT production. Although it is not until 1993 that catalytic chemical vapor deposition (CVD) is applied for carbon nanotube synthesis,<sup>[26]</sup> with the knowledge accumulated in catalyzing carbon fiber growth, CVD rises as the most promising method because of its low price/unit ratio and good control over SWNT density, position and even chirality.

CVD growth of SWNTs involves several elementary steps, such as adsorption and dissociation of carbon precursor molecules on catalyst surface, carbon atom dissolution and diffusion, nucleation and elongation of SWNTs.<sup>[27]</sup> All the steps are tightly related with the catalyst particle, which not only serves as a template

for tube nucleation,<sup>[28]</sup> but also affects the incorporation of carbon atoms for growing SWNTs.<sup>[29]</sup> More importantly, the structure and morphology of the catalyst particle might determine the chirality of SWNT which grows on it.<sup>[30]</sup> Other reaction parameters, such as the carbon precursor, the reaction temperature and the growth pressure, can only affect SWNT growth through modulating the performances of catalysts. In the past two decades, most efforts in chirality selective synthesis of SWNTs have been focused on rational design of catalysts.<sup>[31–35]</sup> So far, high-quality SWNTs with single chirality abundance of over 90% can be attained on well-designed catalysts.<sup>[36–38]</sup>

Despite of the great progress made in chirality selective synthesis of SWNTs, the mechanism for the experiment successes is far from clarification, excluding a possible link establishment between catalyst and SWNT chirality to guide the development of innovative catalysts boosting chirality-specific SWNT synthesis. By combining experimental results and computer simulations, some simplified models are constructed to interpret certain chirality preference. Nevertheless, a whole view of chirality-defined synthesis of SWNTs is still lacking. To fill this gap, in this review, we will first describe the catalytic mechanisms that proposed for SWNT nucleation and growth. Particularly, models involved with SWNT chirality will be addressed to describe the growth thermodynamics and kinetics. How the SWNT–catalyst interface energy and structural match regulate SWNT nucleation and growth rate will be elucidated to establish a general mechanism for chirality-selection growth. With these understandings, the state of the art in chirality-controlled synthesis of SWNTs from diverse experiments will be revisited, and the respective chirality-governing factors will be clarified (Figure 2). Finally, challenges and future opportunities in SWNT synthesis field will be discussed.

## 2. Fundamentals of Catalyst in SWNT Growth

### 2.1. SWNT Growth Models

#### 2.1.1. Base Growth and Tip Growth Model

SWNT growth starts with nucleation from a catalyst particle, which is generally supported by a flat substrate or porous oxide during CVD process. A strong particle–support interaction could anchor the catalyst on the surface, pushing the growing SWNT away from the support when incorporating new carbon atoms to the SWNT rim (Figure 3a). Such a growth model is called “base growth.”<sup>[27]</sup> Catalysts supported on flat surfaces, such as SiO<sub>2</sub>/Si,<sup>[27,39,40]</sup> quartz,<sup>[41–43]</sup> sapphire,<sup>[44–47]</sup> MgO,<sup>[48,49]</sup> or their porous counterparts,<sup>[50,51]</sup> generally trigger SWNT formation by a base growth mode. Under the circumstances, the interaction between catalyst and support is strong enough

to anchor the catalyst and reconstruct the catalyst particle morphology through minimizing its total free surface energy. For example, the equilibrium shape of a supported solid particle follows a Wulff–Kaischew theorem,<sup>[52]</sup> where the Wulff shape is truncated at the particle–support interface and the truncated amount is proportional to the particle–support adhesion energy.

On the contrary, a weak catalyst–support interaction leads to the generation of SWNTs by tip-growth model (Figure 3b). During the elongation process, the catalyst particle residing at the SWNT tip is pushed far away from where the SWNT nucleates.<sup>[53]</sup> Compared with particles lying on surface and spitting SWNTs by base-growth model, the catalysts have more exposed surfaces to the environment and are more difficult to be deactivated by carbon encapsulation, facilitating the growth of ultralong SWNTs on surface by a well-known “kite” mechanism.<sup>[54–57]</sup> In such a case, the equilibrium morphology of catalyst nanoparticles is expected to be similar to that of free nanoparticles. That is, a spherical morphology for liquid catalyst and a Wulff shape for solid one.

The growth model differences arise from the different catalyst adhesion energies on the support, which subsequently

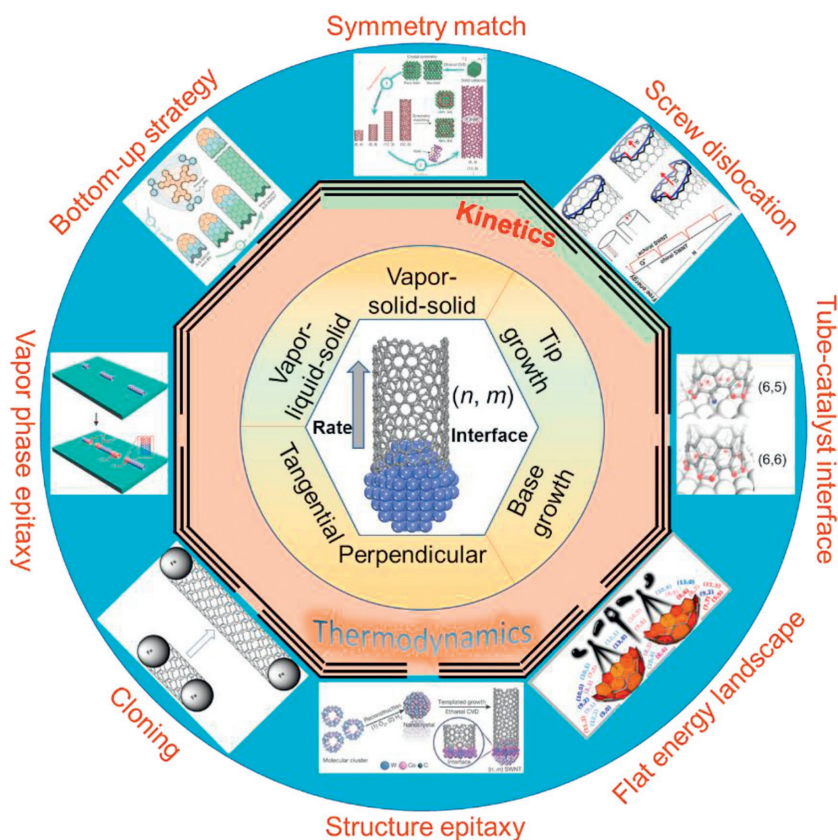


**Figure 2.** SWNT growth mechanisms and approaches to chirality-controlled synthesis of SWNTs. Image attributions: Symmetry match: Reproduced with permission.<sup>[38]</sup> Copyright 2017, Springer Nature. Screw dislocation: Reproduced with permission.<sup>[29]</sup> Copyright 2009, National Academy of Sciences. Tube–catalyst interface: Reproduced with permission.<sup>[83]</sup> Copyright 2014, Springer Nature. Flat energy landscape: Reproduced with permission.<sup>[105]</sup> Copyright 2014, American Chemical Society. Structure epitaxy: Reproduced with permission.<sup>[36]</sup> Copyright 2014, Springer Nature. Cloning: Reproduced with permission.<sup>[128]</sup> Copyright 2006, American Chemical Society. Vapor-phase epitaxy: Reproduced with permission.<sup>[130]</sup> Copyright 2009, American Chemical Society. Bottom-up strategy: Reproduced with permission.<sup>[37]</sup> Copyright 2014, Springer Nature.



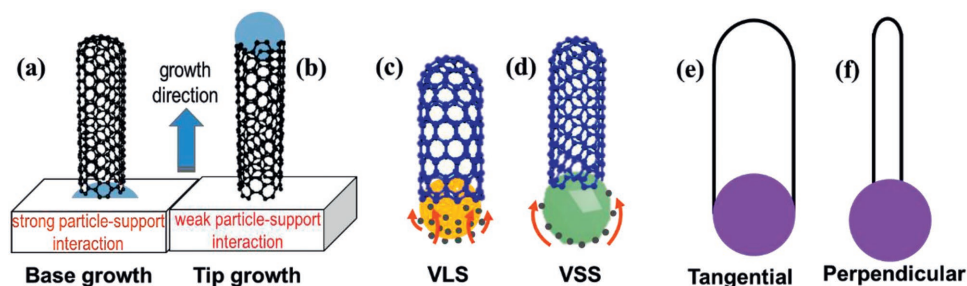


**Figure 3.** Schematic illustration of SWNT growth respectively following: a) base growth model; b) tip growth model; c) VLS mechanism; d) VSS mechanism; e) tangential mode; f) perpendicular mode.

affects catalyst morphology and modifies SWNT nucleation and growth kinetics. Hence, the SWNT chirality distribution can be regulated by controlling the metal–support interactions and the SWNT growth model.<sup>[53,58]</sup> An Fe–Ti–O catalyst, the reduction of which affords the formation of Fe nanoparticles having strong metal–support interactions (SMSI) with the underlying  $\text{TiO}_x$  support, was developed for chiral-selective growth of SWNTs.<sup>[58]</sup> Compared with SWNTs grown on Fe particles in the absence of SMSI, the Fe–Ti–O catalyst tends to synthesize SWNTs with large chiral angles. Based on nanobeam electron diffraction analysis, more than 94% of SWNTs are identified to have chiral angles larger than  $15^\circ$ . The high chiral-angle selectivity is originated from the unique morphology and enhanced wettability of Fe nanoparticle on  $\text{TiO}_x$  support, induced by the SMSI.<sup>[58]</sup>

He et al.<sup>[53]</sup> compared the chirality distributions of Co-grown SWNTs by different models on two  $\text{Co}_x\text{Mg}_{1-x}\text{O}$  solid solutions. One  $\text{Co}_x\text{Mg}_{1-x}\text{O}$  catalyst is prepared by impregnation and affords the growth of SWNTs by base growth model.<sup>[59]</sup> SWNTs grown on the catalyst at  $600^\circ\text{C}$  demonstrate a high selectivity to (6, 5) SWNTs. The other  $\text{Co}_x\text{Mg}_{1-x}\text{O}$  catalyst is obtained by atomic layer deposition (ALD).<sup>[53]</sup> Under identical CVD reaction conditions, the ALD-prepared catalyst also offers the growth of SWNTs but taking a tip growth model. Compared with that of base-growth SWNTs, the chirality distribution of tip-growth SWNTs is broader and the selectivity to (6, 5) species is lower.<sup>[60]</sup> Such a SWNT chirality distribution difference is attributed to the different SWNT growth models, leading to the different morphologies of active Co nanoparticles adopted during SWNT synthesis.

### 2.1.2. Vapor–Liquid–Solid (VLS) and Vapor–Solid–Solid (VSS) Mechanism

Besides nucleating SWNTs, catalyst particles are also involved in other elementary steps for SWNT creation such as carbon diffusion and incorporation to SWNT open-end. Depending on the physical state of catalyst, i.e., whether in liquid phase or in solid phase, the SWNT growth models are classified as VLS mechanism (Figure 3c) and VSS mechanism (Figure 3d). The physical state of catalyst nanoparticle depends on many factors,<sup>[61–66]</sup> including catalyst composition, catalyst size, carbon dissolution, reaction temperature and pressure, catalyst–support interaction, etc. Generally, small-diameter (<5 nm) transition metal (Fe, Co, Ni, Au, Cu, Ag, etc.) nanoparticles are in liquid state at reaction temperatures higher than  $1000^\circ\text{C}$ .<sup>[63]</sup>

While the carbon source cracking temperature (several hundred degrees) ensures the liquid state of catalysts such as In and Ga throughout SWNT growth process.<sup>[65]</sup> During VLS process, dissociated carbon atoms first adsorb on the catalyst surface and dissolve inside the catalyst. The carbon atoms would then diffuse and precipitate to form a SWNT cap of  $\text{sp}^2$  carbon (Figure 3c). Theoretical calculations suggest that the driving force for carbon diffusion is the carbon concentration gradient within the catalyst particle.<sup>[67,68]</sup> Owing to the liquid state of the catalyst, the carbon diffusion could occur through surface diffusion, subsurface diffusion and bulk diffusion.

Similar to VLS, VSS process consists of the elementary steps such as carbon absorption, diffusion and precipitation for SWNT growth. The only difference from VLS mechanism is that the solid catalyst limits the carbon diffusion only on the surface of catalyst (Figure 3d). At relatively low reaction temperatures, most transition metal nanoparticles are in solid state.<sup>[63]</sup> As revealed by in situ environmental transmission electron microscopy (TEM) experiments,<sup>[59,69–75]</sup> the investigated catalyst nanoparticles remain crystalline during carbon nanotube nucleation and growth process, although structural fluctuations are frequently observed. Such structural fluctuation reflects the metal atom creeping in the solid state because of the large forces exerted by the surrounding tube walls. Metal oxide,<sup>[76,77]</sup> metal carbide,<sup>[38,78]</sup> high-melting temperature metals<sup>[79,80]</sup> and their alloys,<sup>[36]</sup> can preserve solid state even at high reaction temperatures. In addition, increasing the catalyst–support interaction increases the melting temperatures of catalyst particle.<sup>[66]</sup>

The physical state difference could cause significant differences in cap formation and carbon incorporation to the open ends of SWNTs, finally affect SWNT chirality distribution. The initial carbon ring formation is correlated with the catalyst surface structure, demonstrating a “template effect” through a dominant occupation of hollow sites.<sup>[81]</sup> The reconstruction of liquid catalyst during SWNT nucleation inhibits the practical utilization of the nanoparticle structure for controlling the nanotube chirality. As reported by Liu et al.,<sup>[82]</sup> atoms in the liquid catalyst can be easily attached to the SWNT open edge and mitigate the energy differences among chiralities, indicating the potential difficulties in bias certain SWNT chirality during nucleation process. After nucleation, the catalyst adapts to SWNT edge with one-to-one termination, the energy cost for creating kinks on SWNT edges are almost zero<sup>[83]</sup> and SWNT growth rate is therefore proportional to its chiral angle.<sup>[29]</sup> In contrast, solid catalyst favors the nucleation of SWNTs having

an epitaxial relationship with the catalyst.<sup>[28]</sup> The energy barrier for incorporating carbon atoms and creating kinks is relatively high because of the difficulty in destroying the contact between SWNT and catalyst.<sup>[83]</sup> Therefore, the SWNT growth rate is correlated with the number of kinks available at SWNT–catalyst interface. In short, the physical state of catalyst particle has important implications for the resultant growth in terms of both thermodynamics and kinetics.<sup>[84]</sup>

### 2.1.3. Perpendicular Growth and Tangential Growth

It has been widely accepted that there is correlation between the diameter of catalyst particle and that of tube nucleated on it. Microscopic correlation between catalyst size and SWNT diameter were revealed by the TEM characterizations.<sup>[27]</sup> Building from the diameter correlations, several groups advance the diameter-controlled growth of SWNTs by controlling the catalyst particle sizes.<sup>[40,85]</sup> However, a systematic TEM investigations of SWNTs grown on Co nanoparticles discriminated two nucleation and growth modes<sup>[86]</sup>: one is tangential model where the tube diameter is close to that of catalyst particle (Figure 3e); the other is perpendicular mode, where the tube diameter is significantly smaller than that of catalyst (Figure 3f). Both modes are observed all along SWNT synthesis by CH<sub>4</sub> CVD and the proportion of each configuration evolves with the reaction time. By depositing SWNT cap on Ni cluster and relaxing, the initial stages of different configurations were mimicked.<sup>[86]</sup> With the addition of carbon atoms, two sequences are demonstrated: one shows the growth of SWNT matching the particle size, a typical configuration of tangential mode; The other shows that SWNT wall can grow perpendicularly to the catalyst surface, i.e., perpendicular mode. The simulations also show that the perpendicular mode involves higher energy barriers and such a configuration's elongation is driven by kinetics effects. In contrast, the tangential mode is favored at conditions close to equilibrium. Consequently, perpendicular configurations are more frequently observed at short reaction time and tangential configurations are dominant when prolonging SWNT growth time.

Further calculations investigated the SWNT–catalyst interactions by evaluating the adhesion energy between carbon walls and the catalyst particle.<sup>[87]</sup> Preliminary results suggest that a low carbon solubility in metal particle favors a stable tangential configuration, while a perpendicular configuration is more stable for a SWNT situated on metal particle with a high carbon solubility. Remarkably, recent result shows that it is possible to regulate SWNT growth mode reversibly by tuning the carbon source during CVD growth, resulting in the formation of SWNT intramolecular junctions.<sup>[88]</sup> Although little chirality information is associated with the different SWNT nucleation and growth modes so far, the results highlight the importance of the tube–catalyst interface in governing SWNT growth.

The diameter ratio variation of SWNT to catalyst particle brings a new freedom for chirality-controlled growth of SWNTs and is clearly a double-edged sword. On the one hand, if one wants to precisely control the diameter and even chirality of SWNTs, it is necessary to first control the SWNT nucleation mode on catalyst particles with similar diameters. On the other hand, particles with

different sizes have different carbon solubilities,<sup>[62]</sup> which initiates nucleation of SWNTs with different diameter ratios between SWNTs and catalysts. Consequently, finely tuning the reaction conditions might lead to the perpendicular growth of SWNTs with high chirality selectivity on catalyst particles without a precise size control.<sup>[89]</sup> Further considering the instability of SWNTs with ultra-small diameters,<sup>[90]</sup> SWNTs with a very narrow diameter/chirality distribution can be obtained when growing SWNTs by perpendicular mode. Such a postulation is applicable for explaining the great success in growing SWNTs with nearly one single chirality in recent years.<sup>[35,36,38]</sup> Particularly, recent work demonstrates that SWNTs grown by perpendicular mode are longer than those grown by tangential mode.<sup>[89]</sup> The observations suggest there is a correlation between SWNT growth mode and length, which would ultimately affect the chirality distributions of SWNTs. **Table 1** summarizes some representative results on chirality-selective growth of SWNTs and the possible mode(s) adopted by the nucleated SWNTs. Despite the progress, a more profound understanding is required for future control on SWNT growth mode, which is a precondition for chirality-controlled synthesis of SWNTs.

## 2.2. Flat End-Cap Energy Landscape

No matter what kind of mechanism the SWNT growth would follow, nucleation of a SWNT always start with a cap creation on catalyst surface. The carbon cap resembles a half fullerene, consisting of a number of hexagons and six pentagons.<sup>[90,105,106]</sup> Once the position of the sixth pentagon is fixed onto the graphene lattice, the structure of the SWNT cap is determined and encodes what unique  $(n, m)$  chirality a nascent SWNT would inherit (**Figure 4a**).<sup>[107]</sup> Various aspects of the cap structures and energetics have been previously addressed.<sup>[90,107,108]</sup> A  $(n, m)$  SWNT can have a number of pentagon patterns compatible with its chirality. In 1999, Brinkmann et al.<sup>[108]</sup> have developed a reliable graph-theoretical method to enumerate the number of the hemi-fullerene caps of SWNTs with diameters smaller than 3 nm. The census of SWNT caps reveals a rather crowded cap population, which grows very rapidly following a power law (Figure 4b). Focused on a handful of  $(n, m)$  SWNT caps, Reich et al.<sup>[90]</sup> showed the arrangement of pentagons in determining SWNT chirality. Based on their calculation results, the cap formation usually obeys the isolated pentagon rule, as introducing adjacent pentagons requires an energy of  $\approx 1.5$  eV per pentagon pair. Such a large formation energy for adjacent pentagons explains the lack of SWNTs with diameters smaller than 0.72 nm in low-temperature CVD. For a specific  $(n, m)$  SWNT, it can have several caps obeying the isolated pentagon rule. If the formation energy of a certain cap is larger than energy available during nucleation, SWNT corresponding to this cap will be prohibited to grow.

Aiming to estimate the intrinsic energies of all possible SWNT caps and establish a quantitative structure-property relation, Penev et al.<sup>[105]</sup> performed a systematic study of cap energetics over the whole range of chiral angles ( $0^\circ$ – $30^\circ$ ) for two sets of SWNTs, corresponding to two diameter constrains:  $d \approx 0.8$  nm and  $d \approx 1.0$  nm, respectively. Through studying a set of more than 4500 caps representing 21 chiralities, it is proved there is no variable correlation between the cap energy and the

**Table 1.** A summary of catalysts and SWNTs grown from them. The possible SWNT growth modes are indicated. Perp., Tan., and Ref. are the abbreviations of perpendicular mode, tangential mode, and reference, respectively.

Catalyst	Catalyst preparation	SWNT ( <i>n</i> , <i>m</i> )	VLS/VSS	Tip/Base	Perp./Tan.	Ref.
CoMo/SiO <sub>2</sub>	Impregnation: cobalt nitrate, ammonium heptamolybdate	(6, 5), (7, 5)	VSS	Base	Perp.	[31]
FeRu/SiO <sub>2</sub>	Impregnation: iron nitrate, ruthenium chloride hydrate	(6, 5)	VSS	Base	/	[33]
FeCo/Zeolite	Impregnation: iron acetate, cobalt acetate	(6, 5), (7, 5)	VSS	Base	/	[32,91]
FeCu/MgO	ALD: iron acetylacetonate, copper acetylacetonate	(6, 5)	VSS	Base	Perp.	[34,92]
CoMn/MCM-41	Isomorphous substitution: cobalt sulfate, manganese sulfate	(6, 5)	VSS	Base	Perp.	[93]
CoPt/SiO <sub>2</sub>	Impregnation: cobalt acetate tetrahydrate, hexachloroplatinic acid hexahydrate	(6, 5)	/	Base	/	[94]
Au/Al <sub>2</sub> O <sub>3</sub> /SiO <sub>2</sub>	Vacuum evaporation, sputtering	(6, 5)	/	Base	/	[95]
Co/SiO <sub>2</sub>	ALD: cobalt acetylacetonate	(6, 5)	VSS	Base	Perp.	[51]
Ni/SiO <sub>2</sub>	ALD: nickel acetylacetonate	(6, 5)	VSS	Base	Perp.	[96]
FeMn/MgO	Impregnation: iron nitrate, manganese acetate tetrahydrate	(6, 5)	VSS	Base	Perp.	[97]
CoCu/quartz	Dip coating: copper and cobalt precursors	(6, 5)	VSS	Base	/	[98]
NixFe <sub>1-x</sub>	Microplasma: nickelocene, ferrocene	(8, 4)	VSS	/	Perp.	[99]
Fe	Thermal decomposition: ferrocene	(13, 12)	VSS	/	Perp.	[100]
Co/TUD-1	Impregnation: cobalt sulfate heptahydrate	(9, 8)	VSS	Base	Perp.	[101]
S-Co/SiO <sub>2</sub>	Impregnation: cobalt acetylacetonate, H <sub>2</sub> S	(9, 8)	VSS	Base	Perp.	[102]
CoxMg <sub>1-x</sub> O	Impregnation: cobalt nitrate	(6, 5)	VSS	Base	Perp.	[53,59]
CoxMg <sub>1-x</sub> O	ALD: cobalt acetylacetonate	(6, 5)	VSS	Tip	Perp.	[53,60]
Fe/SiO <sub>2</sub>	Immersion: iron nitrate	(10, 10)	VSS	Base	/	[30]
W <sub>6</sub> Co <sub>7</sub> /SiO <sub>2</sub>	Impregnation: W <sub>39</sub> Co <sub>6</sub> O <sub>x</sub>	(12, 6), (16, 0), (14, 4)	VSS	Base	Perp.	[36,103,104]
Mo <sub>2</sub> C/Al <sub>2</sub> O <sub>3</sub>	Coating: (NH <sub>4</sub> ) <sub>6</sub> Mo <sub>7</sub> O <sub>24</sub> ·4H <sub>2</sub> O	(12, 6)	VSS	Base	Perp.	[38]
WC/Al <sub>2</sub> O <sub>3</sub>	Coating: (NH <sub>4</sub> ) <sub>6</sub> W <sub>7</sub> O <sub>24</sub> ·6H <sub>2</sub> O	(8, 4)	VSS	Base	Perp.	[38]

chiral angle (Figure 4c).<sup>[105]</sup> Such a flat energy landscape rules out an intrinsic preference to a specific SWNT chirality (*n*, *m*) based on the energetics of the cap alone, thus leaving room for other strategies to control the SWNT chirality.

After a cap becoming mature, the chirality of SWNT is difficult to change.<sup>[106]</sup> Consequently, in pursuit of SWNTs with desired chirality, it is necessary to control the cap structure by controlling the nucleation thermodynamics, relying on the contact interface between the *sp*<sup>2</sup>-carbon lattice edge and the catalyst. In addition, the SWNT growth kinetics, which regulates the SWNT length, could also affect the chirality distribution of the product.

### 2.3. Thermodynamics of SWNT Growth

The chirality of a SWNT becomes permanently “locked in” once a mature cap with six pentagons is fabricated. The formation energy of the nucleus is affected by its interface with catalyst, particularly when nucleating on a solid catalyst.<sup>[28,83]</sup> Such a SWNT–catalyst interaction drives the selective nucleation of SWNTs with a low formation energy. Early experimental work by Zhu et al.<sup>[109,110]</sup> explored the structural correlation between the catalyst and the corresponding SWNT by atomic resolution

TEM. Crystalline face-centered cubic (*fcc*) Co catalyst catalyzes the growth of a SWNT with a chirality of (31, 14) (Figure 5a). Increasing the sample temperature to 700 °C does not change the shape and crystal state of the Co nanoparticle, indicating a stable interface between Co and SWNT. Figure 5b presents a typical SWNT nucleation point at early stage. The lattice fringe is assigned as (1 1 1) plane of *fcc* Co, which acts as a nucleation site for the formation of parallel graphene. As the lattice of a graphene layer fits well with that of the Co (1 1 1) plane (Figure 5c), there is a stable interaction between graphene and Co catalyst. The structural correlation between the graphene and the step edge is highlighted in Figure 5d. It is expected that different angles of step edge on the (1 1 1) plane with respect to growth direction would lead to SWNTs with different chiral angles. All the results indicate that the interface between SWNT and catalyst is quite stable, and the catalyst surface physics may contribute to the chirality definition of synthesized SWNTs.

Pioneer theoretical calculations performed by Reich et al.<sup>[28]</sup> showed that lattice-matched caps and tubes next to Ni surface are more stable than lattice-mismatched structures. In the simulations, all energies are expressed as excess energies compared to a perfect graphite and Ni sheet. The cap growth is modeled as layer by layer growth and the energy per atom in the last layer is calculated. The edge energy comes from



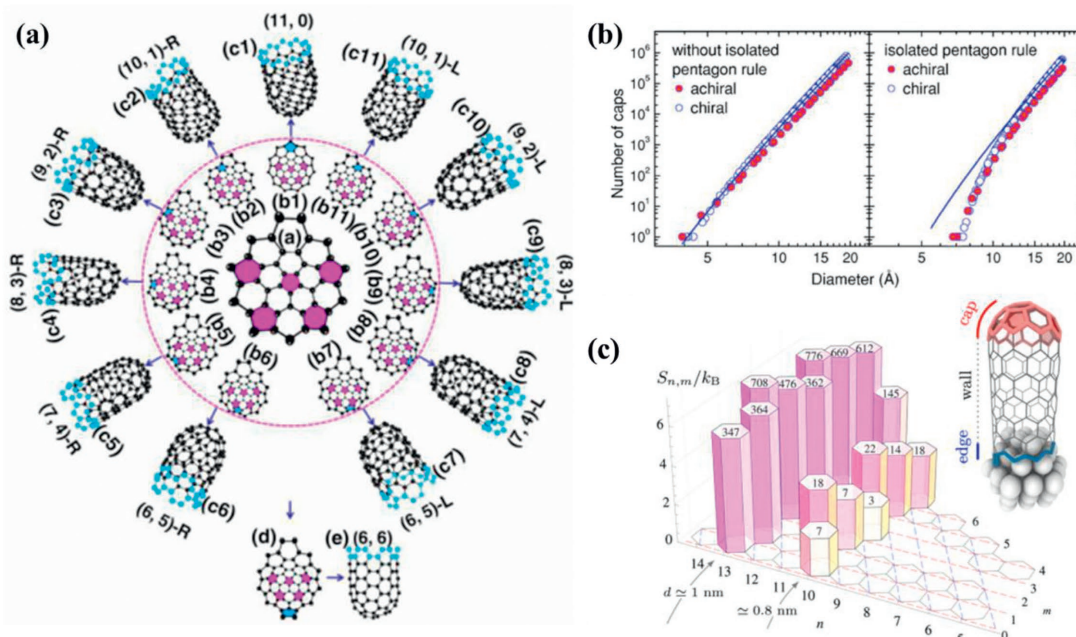


**Figure 4.** a) The nucleation of an SWNT from a graphitic cap with five pentagons. 11 possible mature caps are formed after adding a sixth pentagon. Reproduced under the terms of the CC-BY Creative Commons Attribution 3.0 Unported Licence.<sup>[107]</sup> Copyright 2018, Royal Society of Chemistry. b) Number of all possible carbon caps as a function of tube diameter without (left) and with (right) obeying the isolated pentagon rule. Reproduced with permission.<sup>[108]</sup> Copyright 2005, American Physical Society. c) Configurational entropy  $S_{n,m}$  associated with multiple possible nanotube end-caps with isolated pentagons for the  $(n, m)$  pairs of two sets of SWNTs ( $d \approx 0.8$  nm and  $d \approx 1.0$  nm). The inset shows a schematic presentation of partitioning for SWNT formation on a catalyst particle. Reproduced with permission.<sup>[105]</sup> Copyright 2014, American Chemical Society.

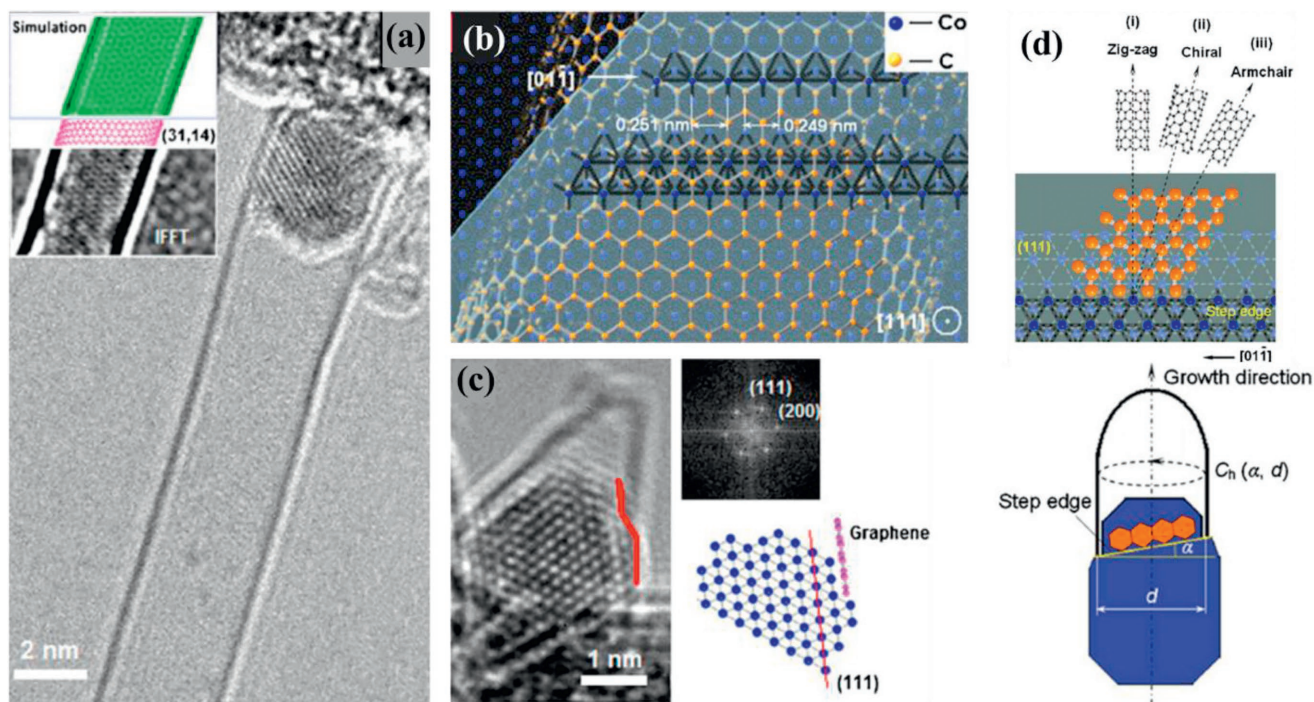


**Figure 5.** a) High-resolution TEM image of SWNT grown from catalytic Co nanoparticle from which the SWNT chirality and Co structure are determined. b) A nucleation model showing the lattice overlapping of graphene over Co (111). c) Co nanoparticle with a step site, which acts as the SWNT nucleation site. Inset shows the corresponding fast Fourier transformation pattern and the atomic model. d) Structural correlation between the graphene and Co (111) plane, showing the formation of SWNTs with different chiral angle (top). Schematic diagram of an SWNT nucleation point (bottom). Reproduced with permission.<sup>[109]</sup> Copyright 2008, Elsevier B.V.

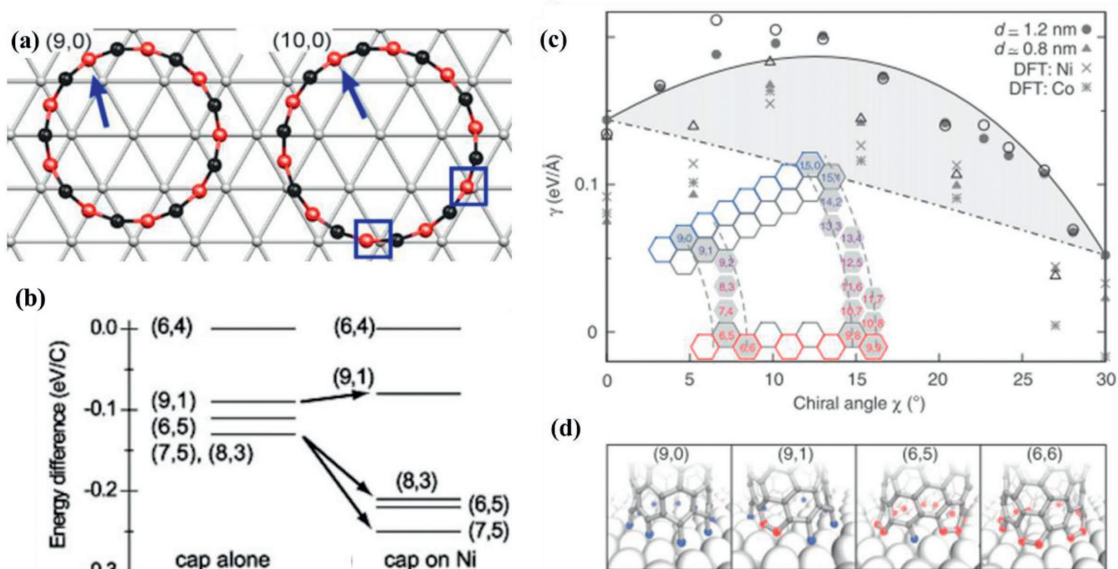


**Figure 6.** a) Lattice matching of (9,0) and (10,0) edge on Ni. Red atoms are edge atoms. The atoms indicated by arrows lie in the stable site, the atoms indicated by squares in the costly site. b) Excess energies per layer for chiral caps without Ni and on Ni (1 1 1). a,b) Reproduced with permission.<sup>[28]</sup> Copyright 2016 Elsevier B.V. c) SWNT–catalyst interface energies calculated for two sets of SWNTs. Static DFT calculations on Ni and Co are also shown. The dash-dotted line corresponds to liquid catalyst. d) Atomic structures for the interface of different SWNTs on catalyst. c,d) Reproduced with permission.<sup>[83]</sup> Copyright 2014, Springer Nature.

two contributions, the cap energy and carbon–metal energy. The cap energy per atom scales roughly as  $d^{-2}$  or the number of hexagons in the cap. For SWNTs with similar diameters, their cap energies are similar.<sup>[105]</sup> The edge energy difference is thus determined by the carbon–metal energy per atom which depends on whether the cap is lattice-matched to the metal surface. For achiral SWNT caps, such a lattice match requires cap match both locally and globally. Because the C–C distance (2.46 Å) is close to the Ni bond length (2.49 Å), local match is fulfilled for any achiral SWNT cap. Both diameter and symmetry of cap are required to match Ni surface in view of global match, which would decrease the carbon–metal energy. For example, a lattice-matched (9, 0) cap decreases the carbon–metal energy by 0.15 eV/C, whereas the non-matched (10, 0) cap increases the carbon–metal energy by 0.07 eV/C (Figure 6a). Consequently, achiral SWNTs that matches the metal surface are favored to nucleate on solid catalyst compared with mismatched achiral SWNTs. Different from achiral SWNTs, chiral SWNTs do not allow a global match but a local carbon–metal match because of their irregular edges. Detailed calculations show that chiral (7, 5), (6, 5) and (8, 3) caps have good local carbon–Ni lattice match, so that they have a low excessive energy on Ni (1 1 1). In contrast, (9, 1) cap has a high excessive energy (Figure 6b) because it does not have a good match on Ni. Overall, the cap edge energy strongly depends on the carbon–metal energy and affects the abundances of different SWNTs.

Subsequent simulations also implied that the catalyst structure strongly correlates with the SWNT chirality selection.<sup>[83]</sup> A flat Ni (1 1 1) slab is also used in the computation to represent the solid catalyst. The contact interface between the  $sp^2$ -carbon lattice and the metal catalyst contains the chirality dependence. Two sets of SWNTs with  $d \approx 0.8$  nm and

$d \approx 1.2$  nm are chosen to investigate the chiral selectivity of nucleation. The SWNT–substrate interface energies calculated by molecular dynamics is shown in Figure 6c. SWNTs with achiral edges form tight low-energy contacts and chiral tubes have a higher interface energy which is roughly in proportional to the number of kinks. The atomistic structures for the (9, 0), (9, 1), (6, 5) and (6, 6) SWNTs are displayed (Figure 6d). Clearly, tubes such as (9, 1) and (6, 5), tend to tilt to reduce the interface energy. The symmetry of such ( $n, 1$ ) and ( $n, n - 1$ ) tubes allows them to tilt off the vertical axis, improving the SWNT–interface contact. For both sets of SWNTs, the bounds of the chiral angle range are energy minima, and the energies of armchair SWNTs are lower than that of zigzag ones. The free energy of the critical nucleus ( $G^*$ ) determines the nucleation probability by the formula  $N(\chi, d) \propto e^{-G^*/k_B T}$ . The nucleation probability falls rapidly with  $\chi$  ( $\chi = \theta$  (chiral angle) near zigzag tube or  $\chi = (30 - \theta)$  for near armchair one). Accordingly, SWNT with a chiral angle of 15° has the largest cap-nucleation energy and unlikely to nucleate, and achiral SWNTs has the favorable cap-nucleation energies.

This way offers a direct chirality-controlled synthesis of achiral SWNTs using catalyst matching on flat planes like Ni (1 1 1). Besides achiral SWNTs, it is possible to match other SWNT species by carefully selecting catalyst surface planes. Recent density functional theory (DFT) simulations by Li's group fit SWNTs of different chiralities on different planes of  $W_6Co_7$  (Figure 7a).<sup>[36,103,104]</sup> The results show that the atomic arrange of the (0 0 12) plane matches well the circumstance of a (12, 6) SWNT (Figure 7b), the nucleation of which is energetically favored. Similarly, (16, 0) SWNT matches the (1 1 6) plane of  $W_6Co_7$  and are more likely to nucleate on  $W_6Co_7$  with plenty of (1 1 6) plane. Therefore, the theoretical results extend



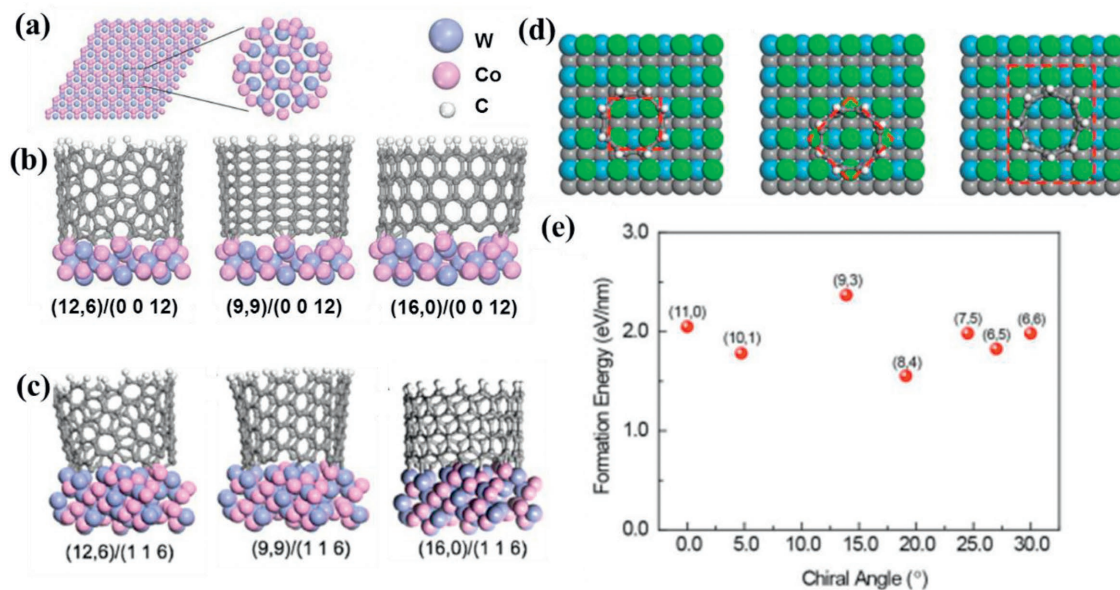


**Figure 7.** a) Vertical view of the catalyst structure of the (0 0 12) plane of the W<sub>6</sub>Co<sub>7</sub> nanoparticle. b) Side view of interfaces between SWNTs with different chiralities and the (0 0 12) planes. a,b) Reproduced with permission.<sup>[36]</sup> Copyright 2014, Springer Nature. c) Side view of interfaces between SWNTs and (1 1 6) planes. Reproduced with permission.<sup>[103]</sup> Copyright 2015, American Chemical Society. d) The high-symmetry relative position of SWNT on WC (100) surface: square, diamond, and rectangle. e) The formation energies of SWNTs with different chiralities on WC (100) surface. d,e) Reproduced with permission.<sup>[38]</sup> Copyright 2017, Springer Nature.

the possibility of growing SWNTs other than achiral species by structure match if the tight contact is dominant.

To go one step further, Ding and co-workers proposed a symmetry match between the SWNT and the catalyst surface in growth thermodynamics.<sup>[38]</sup> The symmetry of a SWNT is determined by chirality indices ( $n$ ,  $m$ ), where the symmetry fold is a common divisor of  $n$  and  $m$ . Therefore, zigzag, armchair and chiral SWNTs could have different symmetries. Based on their simulations, the lowest formation energy is possessed by SWNTs having the same symmetry as the catalyst surface (Figure 7d). For example, SWNT species, as (8, 4), (12, 4), (12, 8) and (16, 8), have a four-fold symmetry, which is similar to the quasi four-fold symmetry of the (1 0 0) plane of WC. Consequently, the nucleation probability of these SWNTs are high on WC (1 0 0) surface because of their lower formation energy compared with SWNTs do not have a four-fold symmetry (Figure 7e). Overall, the SWNT–catalyst interface affects the energy of the SWNT nucleus, which governs the nucleation probabilities of different SWNT species. The nucleation thermodynamic suggests a direct chirality control by regulating SWNT nucleation on catalyst surface.

#### 2.4. Growth Kinetics of SWNTs

Besides nucleation thermodynamics, SWNT growth kinetic, which rules the lengths of the SWNT, could also affect the abundances of different SWNT species. SWNTs with greater lengths (or rates) will be translated into a greater number of fragments during sonication process and have more opportunities to be characterized, contributing to their larger abundances. On the contrary, SWNTs which can nucleate on

catalyst but with negligible growth rates, are unlikely to be detected because of their ultrashort length. To investigate the SWNT growth kinetic, the sequential steps for SWNT growth should be recalled and the threshold step for SWNT elongation must be identified. The process for the elongation of a SWNT can be divided into three steps: carbon feedstock dissociation, carbon atom diffusion and incorporation of carbon atoms into the open ends of SWNT.<sup>[111]</sup> In the following, the energy barriers for each step are addressed and compared.

##### 2.4.1. Carbon Source Dissociation

Catalytic decomposition of carbon sources, include C<sub>2</sub>H<sub>2</sub>, CH<sub>4</sub> and CO, which are the commonly used carbon sources for SWNT synthesis, have been extensively studied.<sup>[111–114]</sup> Owing to the presence of catalyst, the barrier for carbon source dissociation is greatly decreased compared to that in vacuum. Using ab initio plane wave density functional calculations, Hofmann et al.<sup>[111]</sup> studied the dissociation energy for C<sub>2</sub>H<sub>2</sub> and CH<sub>4</sub> on the most stable Ni (1 1 1) surface. The calculated energy barrier for H abstraction reaction of C<sub>2</sub>H<sub>2</sub> on Ni is 1.4 eV. For comparison, the dissociation barrier for an isolate C<sub>2</sub>H<sub>2</sub> molecule is 5.58 eV, highlighting the importance of catalyst effect in lowering the activation energy. Similar to flat Ni surface, the stepped Ni (1 1 1) can also lower the energy barrier for C<sub>2</sub>H<sub>2</sub> dissociation with an energy barrier of 1.3 eV. However, the step edge in Ni (1 1 1) does not promote the C<sub>2</sub>H<sub>2</sub> dissociation significantly because the strong bonding of reaction intermediates at the step blocks the adsorption of new reactant molecules. The energy barrier for CH<sub>4</sub> dissociation on Ni (1 1 1) is smaller than dissociating C<sub>2</sub>H<sub>2</sub>. The calculated energy barrier for CH<sub>4</sub>

dissociation on Ni (1 1 1) step edge and flat surface is 0.9 eV and 1.2 eV, respectively.<sup>[111]</sup> Using first-principles calculations, Sorescu et al.<sup>[114]</sup> investigated CO decomposition on Fe surface. Starting from a fourfold configuration, two paths for CO dissociation on Fe (1 0 0) are considered. One path corresponds to a sequential mechanism where the C atom remains at the original site, but the CO bond is stretched continuously, and the O atom finally migrates to a neighboring four-folded sites. The energy barrier for such a dissociation path is 1.06 eV. In the second path, CO dissociation follows a concerted mechanism where both the C and O atoms are moving away from each other with a dissociation energy barrier of 1.22 eV. Despite of the possible differences in the values for carbon source dissociation from different calculation methods, the dissociation energy barriers on transition metals are generally smaller than 1.5 eV.

#### 2.4.2. Carbon Diffusion

The dissociated carbon atoms could adsorb and even dissolve inside the catalyst particle, diffuse toward to the rear end of catalyst, leading to the nucleation and the growth of SWNTs. The carbon diffusion for SWNT growth is analogue to that for synthesizing carbon fibers by CVD.<sup>[115–118]</sup> Baker et al.<sup>[115]</sup> proposed a “classical” VLS growth model for dissociated carbon atom diffusion to form carbon fibers. They suggest that the heat generated from carbon source dissociation on catalyst surface causes a temperature gradient, driving the carbon diffusion through catalyst. The respective activation energy for carbon diffusion in bulk Fe, Co and Ni is 0.71 eV, 1.5 eV and 1.5 eV. The bulk diffusion energies are close to the activation energies for carbon fiber synthesis, suggesting that the carbon diffusion could be the rate limiting step for carbon fiber growth. However, not all the surface reaction on catalyst is exothermic and the temperature gradient is not necessarily the driving force. Subsequently, Rostrup-Nielsen et al.<sup>[117]</sup> pointed out that the driving force for carbon diffusion is the carbon concentration gradient, arising from the different carbon activities between the fiber/catalyst interface and the catalyst surface where the carbon decomposition takes place. On the basis of kinetic results for carbon deposition and gasification on many metal catalysts, a new model where the dissociated carbon atoms could diffuse rapidly through the surface carbide was proposed.<sup>[118]</sup> In the steady state growth period, the carbon concentration gradient is maintained to migrate carbon atoms to the rear end of the catalyst particle. Assisted with environmental TEM observations on carbon nanotube growth, Helveg et al.<sup>[69]</sup> performed DFT calculation on the transportation of carbon atoms along the graphene and Ni interface. The energy required to move carbon atom on Ni (1 1 1) surface from a step to a terrace site is only  $\approx 0.7$  eV, suggesting that surface diffusion is more favorable for carbon nanotube growth. Using DFT calculations on slab models of the catalyst-carbon system, Hofmann et al.<sup>[70]</sup> revealed the low activation energy path for carbon diffusion. For surface diffusion, the initial stable carbon absorption site on the Ni (1 1 1) surface is the hollow site where carbon is bonded to three Ni atoms. After surface diffusion, the carbon is bonded to two Ni atoms in transition states. The determined energy barrier for

surface diffusion of carbon on Ni (1 1 1) is found to be 0.4 eV, similar to that on Co (1 1 1) surface (0.5 eV). Compared to the energy barrier for carbon bulk diffusion ( $\approx 1.5$  eV on Ni),<sup>[115]</sup> the surface diffusion of carbon atoms is energetically favored for carbon nanotube growth.

Yazyev et al.<sup>[119]</sup> further modeled the carbon diffusion and SWNT growth on different metals (Ni, Pd, Pt, Au, Cu, and Ag). Using first-principles calculations, the binding and diffusion of carbon atoms and dimers, initially produced from carbon source decomposition, on the metal nanoparticle surface and interior are investigated. On coinage metal surfaces (Au, Cu, Ag), the surface dimers are more stable than monoatomic carbon. As dimers located in subsurface and bulk are highly unstable, only surface dimers are involved in the diffusion process. At variance, on the surface or subsurface of late transition metals (Ni, Pd, Pt), atomic carbon could have the lowest chemical potential. For the surface adatom diffusion on Ni (1 1 1), the lowest energy barrier is calculated to be 0.39 eV. In contrast, the energy barrier for adatom diffusion on coinage metal surface is extremely low, only 0.07 eV for Cu and 0.20 eV for Ag. Subsurface and bulk diffusion, which occurs via hopping of interstitial carbon atoms between voids, generally have a higher energy barrier than for adatom diffusion. While for metals with large lattice constants, the activation energy for subsurface diffusion could be smaller than that for surface diffusion. Compared with bulk diffusion, subsurface diffusion always has lower energy barrier because of the smaller elastic response in nanoparticle subsurface. In addition, the surface dimer diffusion barriers are comparable to those for surface adatom diffusion. All the results suggest that bulk diffusion is energetically unfavorable for carbon atom diffusion. Instead, surface diffusion and subsurface diffusion should be dominant during SWNT nucleation and growth. Overall, the driving force for carbon diffusion on surface or subsurface is the carbon concentration gradient and the diffusion energy barriers are generally smaller than 1.2 eV.

#### 2.4.3. Carbon Atom Incorporation into Tube Rim

Because of the high activity of the SWNT open end and the exothermal reaction of incorporating carbon atoms into a tube wall, the barrier for carbon atom incorporation into the tube wall had been thought as very low.<sup>[69,111]</sup> An energy barrier of 0.4 eV was reported to incorporate the carbon atom under the graphene sheet.<sup>[69]</sup> By placing an additional carbon atom at a nearby hollow site of graphene lying on a Ni (1 1 1) surface, Hofmann et al.<sup>[111]</sup> found that the carbon atom joins the graphitic structure spontaneously upon relaxation. However, the simultaneous removal of metal atoms from metal surface is overlooked in the previous work.<sup>[111]</sup> Using DFT calculations, Ding et al.<sup>[113]</sup> carefully calculated the energy barrier for incorporation carbon atoms into a SWNT wall through the tube–catalyst interface, which is modeled as a graphene edge attached to a metal step. **Figure 8a** present the process of incorporating the first carbon atoms into a tube wall attached to a step of the Ni (1 1 1) surface. The lowest path for carbon migration to reach the armchair site of the graphene edge is through the subsurface diffusion with a barrier of 1.02 eV (Figure 8b). As

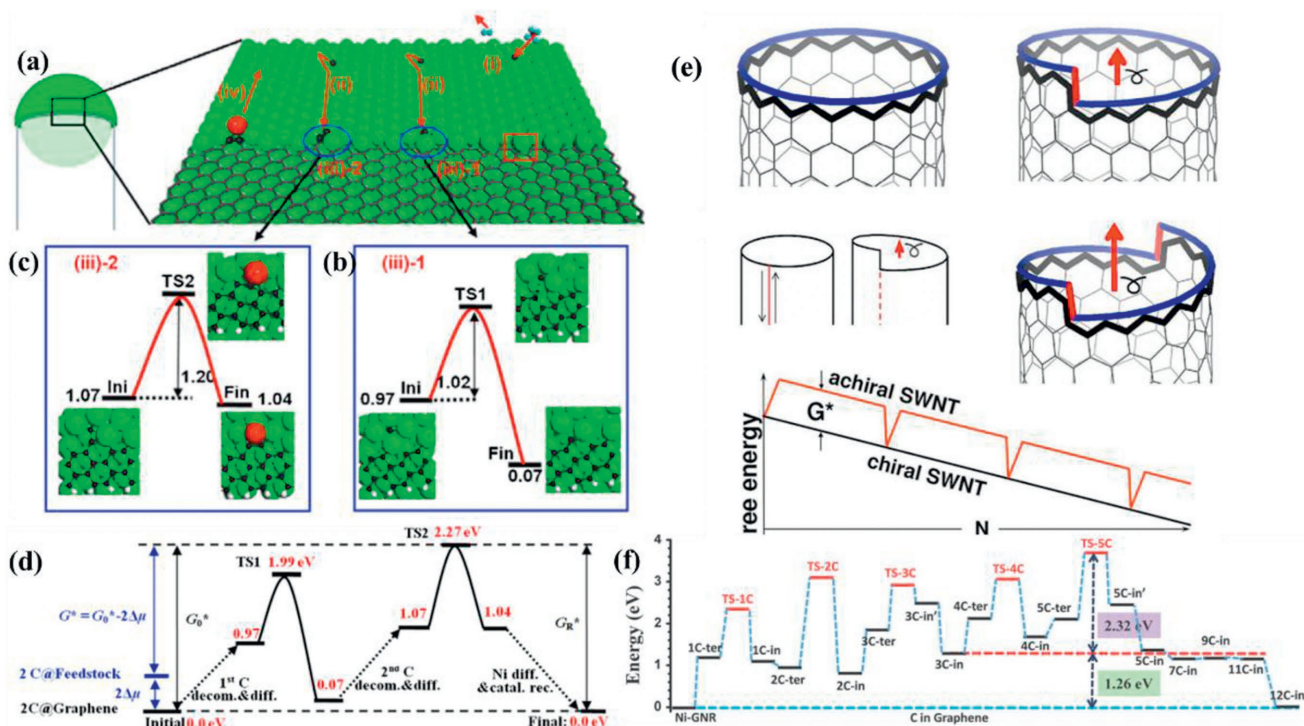


**Figure 8.** a) An interface of graphene-stepped Ni (1 1 1) surface, applied to model a fraction of the SWNT–catalyst step interface. Four steps are involved in the incorporation of carbon atoms: i) carbon feedstock molecule dissociation; ii) carbon atom diffusion; iii) direct incorporation of b) the first carbon and c) the second carbon atoms into the six-membered-ring; iv) a reconstruction of the catalyst induced by metal atom removal. d) Energy profile for incorporating two carbon atoms into graphene on Ni (1 1 1) surface serially. a–d) Reproduced with permission.<sup>[113]</sup> Copyright 2011, American Physical Society. e) An axial screw dislocation in SWNT and free energy profile during the growth of chiral and achiral SWNTs. Reproduced with permission.<sup>[29]</sup> Copyright 2009, National Academy of Sciences. f) Energy profile of a cycle of zigzag SWNT growth on Ni. Reproduced with permission.<sup>[122]</sup> Copyright 2015, Wiley-VCH.

there is no much space for accommodating two carbon atoms, the incorporation of a second carbon atom simultaneously leads to the removal of one Ni atom, which need to overcome a significant high energy barrier of 1.20 eV (Figure 8c). Repeating these cycles leads to the growth of SWNTs with an overall barrier of 2.27 eV (Figure 8d), that is, the energy of the transition state of the second carbon atom insertion using graphene as the reference. Similarly, from the energy profiles of carbon atom incorporation into the SWNT wall on Co (1 1 1), the energy barrier is calculated to be 2.28 eV. Compared with Co and Ni, the absorbed carbon atom on the Fe surface has a lower formation energy because of the high affinity of Fe with carbon atoms. The strong carbon atom affiliation on Fe facet leads to a drop in the overall energy barrier, which is calculated to be 1.85 eV.<sup>[113]</sup> When comparing the calculated barriers for carbon feedstock decomposition (<1.5 eV) and carbon atom diffusion (<1.2 eV), the carbon atom insertion into the SWNT rims could be the threshold step for SWNT growth.<sup>[113]</sup>

#### 2.4.4. Screw Dislocation Theory for SWNT Growth

After the six-pentagon nucleus formation, a strong interaction between the hemispherical cap and the catalyst nanoparticle is essential to maintain the open end of the SWNTs.<sup>[120]</sup> Incorporating carbon atoms into the open ends of SWNTs could

be the threshold step for the elongation of SWNTs. Considering the periodic makeup and crystal attributes of carbon nanotubes, Ding et al.<sup>[29]</sup> suggested that SWNT growth also obeys the screw dislocation model established for crystal growth, where a significant barrier should be overcome before nucleating a new crystal plane on top of a previously completed one (Figure 8e). For a sequential accretion of atoms along the spiral lattice, a screw dislocation provides a non-barrier path.<sup>[121]</sup> In this regard, achiral SWNTs are special and their circular end-edge is entirely uniform, representing a stack of complete atomic rings and resembling to a low-index crystal plane. A comprehensive study on the growth kinetics of zigzag SWNTs were carried out on four different catalysts: Ni, Fe, Co and Cu.<sup>[122]</sup> The calculations demonstrate that the growth is a stepwise process involving the nucleation of a hexagon and the formation of a complete hexagonal ring on the zigzag rim. The nucleation of a stable hexagon is the rate-limiting step for zigzag SWNT growth with a barrier of 3.58 eV (Figure 8f). Such an energy barrier is as high as the formation energy of stable nucleus. Under common CVD conditions, the growth rate of zigzag SWNTs is thus very low, explaining the lack of zigzag SWNTs in products synthesized by CVD. Consequently, the SWNT growth kinetics does not make any positive contribution to bias zigzag SWNTs during growth. In the respect of initiating a new carbon ring at the SWNT rim, the armchair SWNT is similar to zigzag one. However, different from zigzag SWNTs, the energy barrier for



restarting a new armchair ring is rather low.<sup>[29]</sup> For an armchair edge on catalysts such as Fe, Co, and Ni, the calculated energy barrier for carbon incorporation is about 0.06, 0.12 and 0.14 eV, respectively.<sup>[29]</sup> Therefore, armchair SWNTs could grow ring by ring almost unobstructed by the difficulties of re-initiation and with a relatively high velocity.

A chiral ( $n, m$ ) SWNT has  $m$  kinks at the tube rim, serving as the active sites for carbon incorporation. The  $m$  kinks at tube rim are similar to the rim structure of an armchair SWNT so that the growth behavior of a chiral SWNT resembles that of an armchair one. The kinks in ( $n, m$ ) tube readily accrue new carbon atoms with a rate of  $k_0$ . The total carbon deposition rate  $K = k_0 \cdot m$ . Based on the basic characteristics of SWNT chiral angle, the SWNT growth rate ( $R$ ) is proportional to  $m/D$

$$R \sim K/D \sim k_0 \sin \theta \sim \theta \quad (1)$$

where  $D$  is the tube diameter and  $\theta$  represents the tube chiral angle.

Dumlich et al.<sup>[123]</sup> studied the geometric constraints for the addition of carbon atoms to the rim of a growing SWNT, and a growth rate dependence on the SWNT chirality is also revealed. With the aim to validate the above theories and investigate the growth rates of SWNTs with different chiralities, Rao et al.<sup>[124]</sup> performed in situ Raman spectroscopy and compared the SWNT growth rates with their chiral angles. In their experiments, SWNT growth takes place in a laser-induced CVD coupled to a Raman spectroscopy. The SWNT growth rate is deduced from the integrated G band intensity, which is fit by a self-exhausting exponential equation. Postgrowth characterizations are carried out to confirm that the Raman signals are from an individual SWNTs and SWNT chirality is identified from the radial breathing mode. By making chiral index assignments for nine SWNTs and plotting the growth rate as a function as chiral angle, a positive correlation between linear growth rate and the SWNT chiral angle is evident, showing a good agreement with the dislocation theory. However, not all the experimental results agree with the dislocation theory. He et al.<sup>[89]</sup> performed systematic TEM investigations on SWNTs synthesized from Fe nanoparticles and found that there is no positive correlation between SWNT length and chiral angle. Instead, SWNT length depends more on the growth mode, i.e., the tube–catalyst interface, which is neglected in the screw dislocation model. The existence of experimental results which are contradictory to the screw dislocation theory rules out it as a general model for SWNT growth, some preconditions must be satisfied before validating the model.

#### 2.4.5. SWNT Growth Kinetic on Solid Catalyst

In the screw dislocation theory, the energy cost for creating a pair of kinks on the armchair edge is calculated to be near zero.<sup>[29]</sup> This is the case for catalyst in liquid state, which adapts to the SWNT edge with a one-to-one termination. In contrast, it is difficult to create a pair of kinks on a solid catalyst surface because of the perfect contact between the armchair SWNT and the catalyst surface. To investigate the SWNT growth rate on solid catalyst, Artyukhov et al.<sup>[83]</sup> augmented the screw

dislocation model by including the kinks created by thermal fluctuations on armchair and zigzag edges, and accounting for the energy penalty  $\approx 1/d^2$  from the wall curvature. The energy cost for creating a pair of kinks on SWNT edge has a noticeable magnitude, and the dependence becomes bimodal with minima for achiral SWNTs and maximum for ( $2m, m$ ) SWNT with a chiral angle of  $19.1^\circ$ . The computations pertaining to the growth kinetics are summarized in Figure 9a (dashed). The energy changes with the addition of a new row of carbon atoms for (6, 6), (9, 9) and (9, 0) SWNTs are presented in Figure 9b. Because of the constantly changing SWNT tilting angle, all three curves depart from the “nucleation to kink flow” scenario of graphene.<sup>[125]</sup> Interestingly, the heights for the first dimer addition and the maximum heights closer to the end are essentially the same for both armchair curves. The zigzag curve bears the same qualitative character, having an initial and a final maximum. With the addition of a new layer of carbon atoms, the system cycles and  $\Delta G$  return to 0. The maximum height of each curve represents the energy barrier to overcome for adding a new row of hexagons,  $\Delta G_A \approx 1.67\text{--}1.86$  eV,  $\Delta G_Z > 3$  eV. Compared with chiral SWNTs (green line in Figure 9b), these energies penalize zigzag and armchair SWNTs and thus sufficiently remove them from the product. Figure 9c shows the configurations for adding the first dimer to the (6, 6) and (9, 0) SWNTs. The concentrations of different site types-Z (zigzag), A (armchair) and K (kink) as a function of chiral angle are presented in Figure 9d. Figure 9e shows the SWNT growth rate. The SWNTs growing the fastest on solid catalyst have chiral angle of  $19.1^\circ$ , corresponding to ( $2m, m$ ) SWNTs. Although zigzag and armchair SWNTs are promoted at high reaction temperatures because of the favored kink formation, under realistic conditions, where  $k_B T \ll \Delta G$ , the growth rates of them are negligible. In addition, for SWNTs with small diameters, the curvature of the wall penalizes the insertion of carbon atoms into SWNT edges.

#### 2.5. Origin of SWNT Chirality Selection

Concerning SWNT growth on liquid catalyst, its structural mobility flattens the cap energy landscape and makes the kinetic route of selection dominant. As the energy for creating kinks on armchair edge is near zero, the SWNT growth rate is proportional to the SWNT chiral angle.<sup>[29]</sup> Assuming the lifetimes of the catalyst particles are identical for all the growing SWNTs, armchair and near armchair SWNTs with large chiral angles are supposed to have greater lengths. The screw dislocation model predicates a respective yield of 11%, 33% and 56% for SWNTs in chiral angle ranges of  $0^\circ\text{--}10^\circ$ ,  $10^\circ\text{--}20^\circ$ , and  $20^\circ\text{--}30^\circ$ , which explain the overall dominance of SWNTs in some products.<sup>[29]</sup> Particularly, such a theory fits well the chirality distributions of SWNTs from HiPco<sup>[126]</sup> and arc-discharge.<sup>[127]</sup> However, by optimizing the SWNT–catalyst interface, thermodynamically optimized SWNT structures can also be realized.<sup>[106]</sup>

When growing SWNTs on solid catalyst, both the kinetics and thermodynamics should be considered concurrently. The population of a specific SWNT in the final products can be estimated by the formula

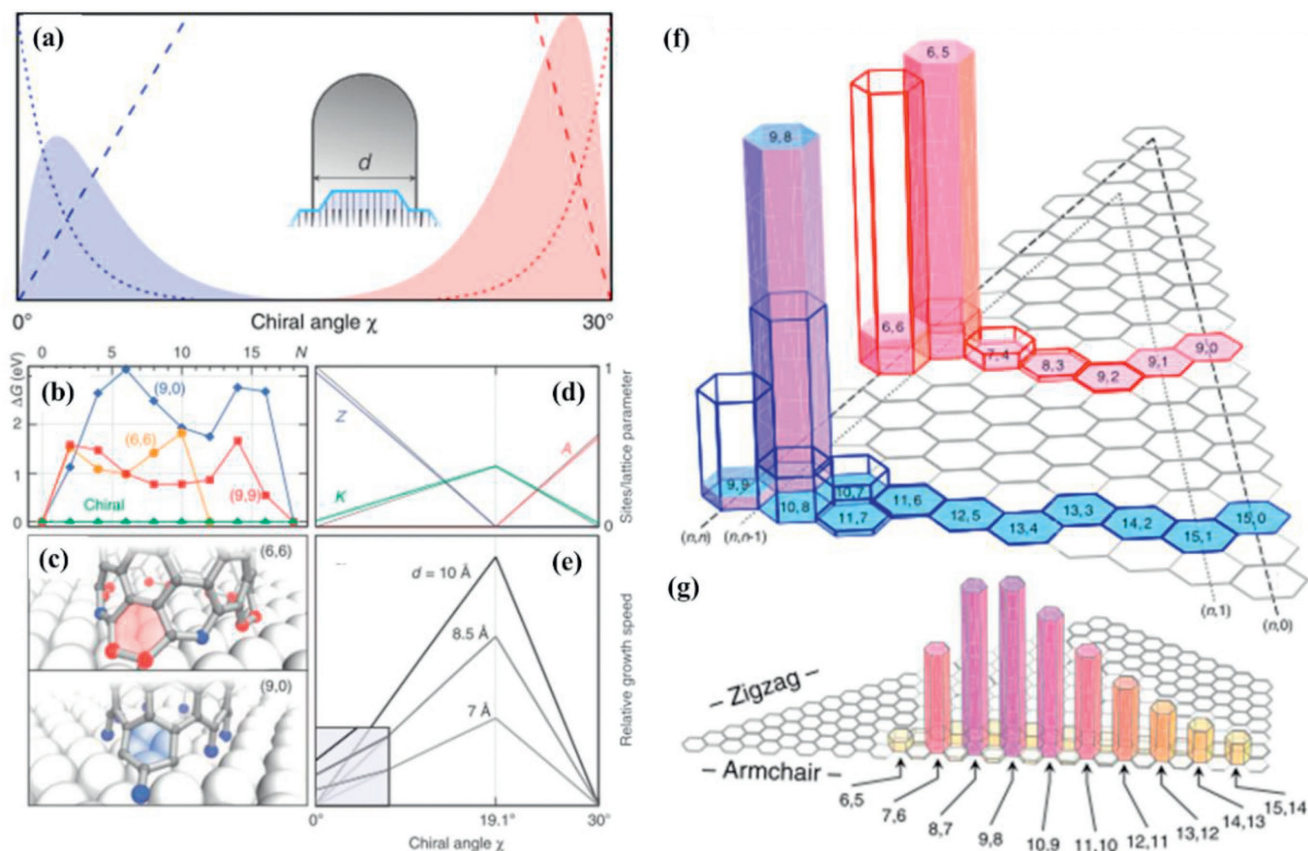


**Figure 9.** a) The abundance distributions computed as the product of nucleation (dotted) and growth rate (dashed) for near-armchair and near-zigzag chiralities. The inset illustrates a nascent SWNT on solid catalyst. b) Free-energy profiles during the growth of a new ring of hexagons on (red, orange) armchair (A) and (blue) zigzag (Z) edges against the number of added atoms. c) The atomic configurations after incorporating first dimer. d) Linear density of different site types on tube edges as a function of chiral angle. e) The growth rate as a function of chiral angle for SWNTs with different diameters. f) Predicated SWNT chirality distribution for two sets of SWNTs ( $d \approx 0.8$  nm and  $d \approx 1.2$  nm) for liquid (empty bars) and solid catalyst (solid bars). g) Full  $(n, m)$  distribution based on an analytical fit to interface energies calculated by molecular dynamics. Reproduced with permission.<sup>[83]</sup> Copyright 2014, Springer Nature.

$$P = N \times R \quad (2)$$

where  $N$  and  $R$  are the nucleation density and growth velocity of the SWNT, respectively. As creating a pair of kinks at armchair edge costs energy, the fastest growing SWNTs are  $(2m, m)$  species and have chiral angle  $\chi = 19.1^\circ$ . Achiral SWNTs, which are kinkless at edges, have low nucleation barriers on solid catalyst. At a given diameter, the SWNT abundance distribution as the product of nucleation and growth rate is computed and presented in Figure 9a. Assuming equal interface energies and growth barriers, the two distributions for near armchair and near zigzag angles are observed. When taking the chirality-dependent SWNT–catalyst contact energies into account, a strong preference to  $(n, n - 1)$  SWNTs are seen for two sets of SWNTs with different diameters (Figure 9f). At  $T = 900$  K, the SWNT chirality distributions show predominant growth of  $(6, 5)$  or  $(9, 8)$  SWNTs on solid catalyst. Through interface energy fitting, a general  $(n, m)$  distribution is computed and presented in Figure 9g. The competition between the interface energies of SWNT with different diameters accounts for the peak in diameter distribution. Further constraint on SWNT

diameter by controlling catalyst size would obtain only a slice of Figure 9g with prominent  $(n, n - 1)$  peaks.

Other than achiral SWNTs, there is possibility that a solid catalyst template exactly matches a certain  $(n, m)$  SWNT. Therefore, the  $(n, m)$  SWNT is favored to nucleate because of its low cap formation energy on the catalyst. As long as the SWNT has a non-zero growth rate, the way catalyst–matching offers a direct chirality control. However, if the energy required for incorporating new carbon atoms into the SWNT–catalyst interface is too high, the growth rate of perfectly matched  $(n, m)$  SWNT will be very low, resulting in SWNTs too short to be detected by either optical or electron microscopy techniques. In such a case, one-index-off SWNTs  $(n, m \pm 1)$ , allowing for rapid kinetics at the cost of higher energy of the contact and nucleation are likely favored. The enrichment of such single-kink SWNTs arises from one distinction that their symmetry allows them to tilt off the vertical axis to improve the interface contact, enabling a substantial closure of the gap between tube edge and substrate. To wrap all this up, if the  $(n, m)$  SWNT exactly match the catalyst template, SWNTs with one index off, like  $(n, m - 1)$  SWNT, could be favored to grow with a high abundance.

Therefore, the origin of SWNT chirality can only be understood when combining both kinetics and thermodynamics. The thermodynamic nucleation barrier is low for SWNTs well matching catalyst surface structures. The growth kinetics is aided by the available kinks at the tube edge and thus favors the chiral ones on solid catalyst and armchair ones on liquid catalyst. The understandings are sufficient for comprehending the disparate experimental results achieved over the past decades.

### 3. Achievements on the Chirality-Selective Growth of SWNTs

Progresses, particularly some recent breakthroughs, have been made in synthesizing SWNTs with controlled chirality. As the SWNT–catalyst interface rules SWNT thermodynamics and kinetics, approaches that can modify the interfacial energies and the incorporation of carbon atoms into SWNT rims would affect abundances of different SWNT species. In the following, the strategies in achieving chirality-controlled growth of SWNTs are addresses and the origins for the chirality selection are explored in the frame of thermodynamics and kinetics.

#### 3.1. Chirality Selection from Thermodynamic Control

##### 3.1.1. Synthesis of SWNTs by “Tandem Plate” CVD

Thermodynamically, SWNTs with a low tube–catalyst interfacial formation energy and a stable tube–catalyst interface have a high possibility of being synthesized. By changing SWNT chirality and further optimizing the tube–catalyst interface during CVD growth process, it is predicated to realize a thermodynamically optimized SWNT structures. Guided by the predication, Zhao et al.<sup>[106]</sup> developed a CVD process allowing the change of SWNT chirality multiple times by periodically alternating the reaction temperatures, which is named as “tandem plate” CVD (TPCVD). Through this process, an enrichment of (15, 2) SWNT and a large abundance of SWNTs with chiral angles smaller than  $10^\circ$  (>70%) are obtained. The enrichment of small-chiral-angle SWNTs is attributed to the chirality change during the TPCVD process. To evaluate the interfacial formation energies between SWNTs and catalysts (Fe, Co, and Ni), DFT calculations are performed. Among all the possible SWNTs with similar diameters, SWNTs with chiral angles smaller than  $10^\circ$  have significantly lower interfacial formation energy than large-chiral-angle SWNTs on all the three catalysts. Meanwhile, SWNT intermolecular junctions with small chiral angle change ( $<5^\circ$ ) have low formation energy. Consequently, such a TPCVD can transform SWNTs with large chiral angles into small-chiral-angle tubes step by step, leading to the enrichment of thermodynamically preferred near zigzag SWNTs. The TPCVD strategy might be extended to achieve other SWNTs with low SWNT–catalyst interfacial formation energy by careful catalyst design and growth condition optimization. However, as the SWNT growth following a VLS mechanism, the structural instability of the liquid catalyst does not allow a very high chirality selection.

##### 3.1.2. Synthesis of SWNTs by Template Molecules

Different from liquid catalyst, solid catalyst can act as the “template” or “seed” for growing SWNTs with low cap formation energy. To grow SWNTs with desired ( $n$ ,  $m$ ), it is necessary to choose suitable “seed,” which can be catalyst particles docked inside short SWNTs, as proposed by Smalley et al.<sup>[128]</sup> In the “cloning” approach, SWNTs are first cut into many short segments and attached with Fe nanoparticles, which are subjected to further CVD process and amplified into long ones inheriting the chirality of the short parent SWNTs (Figure 10a). As a proof-of-concept, end-functionalized HiPco SWNTs with anchor Fe nanoparticles are applied for CVD growth. A short ( $\approx 200$  nm) SWNT segment with docked Fe nanoparticle is amplified into a 6.7  $\mu\text{m}$  long tube (Figure 10b). Such a tube growth occurs bidirectionally and the produced SWNT has a same diameter as the “seed,” suggesting an amplification of the original SWNT, although chirality inheritance of the amplified SWNTs remains to prove.<sup>[129]</sup>

Using the concept of “cloning,” Zhang et al.<sup>[130]</sup> developed a rational approach to grow SWNTs by an open-end growth mechanism. Different from the above approach, the short SWNT segments cut from long SWNTs would be directly served as seeds/catalysts in SWNT cloning. Without addition of metal catalysts, continued SWNT growth from the parent SWNT are observed (Figure 10c). The duplicated SWNTs have the same diameters and chiralities as the parent SWNTs, as verified by the same radial breathing mode frequency for both parent and duplicated SWNTs (Figure 10c). By optimizing the growth conditions, a “cloning” yield as high as 40.7% can be achieved. This work not only verifies the chirality inheritance of duplicated SWNTs, but also helps understand the “cloning” mechanism of open-ended SWNTs.

Such an open-end growth mechanism was later defined as vapor-phase-epitaxy (VPE) and well described by Zhou et al.,<sup>[131,132]</sup> who used single chirality SWNT seeds for amplification. The essence of VPE is achieved by covalent addition of  $\text{C}_2\text{H}_2$  and  $\text{C}_2\text{H}_4$  at the SWNT edge, following Diels–Alder reaction for the generation of six-membered rings. Three exemplary chirality-pure (7, 6), (6, 5), and (7, 7) SWNT seeds with purities up to 90% are initially applied as seeds for cloning (Figure 10d). Through the VPE process, seed SWNTs are significantly elongated, ended in SWNTs with lengths up to tens of micrometers. Both Raman analysis and electrical measurement confirm that the original SWNT serves as a template and encodes the chirality of cloned SWNT. Subsequently, VPE cloning of other SWNT species, such as (9, 1), (8, 3), (10, 2), and (6, 6), were also investigated.<sup>[132]</sup> The work combines SWNT separation with synthesis to achieve controlled growth of nanotubes with preselected chirality and deepens the understandings of chirality-controlled growth of SWNTs.

Similar to short SWNT segments, opened fullerene caps were also adopted for the templated growth of SWNTs via the open-end growth mechanism.<sup>[133]</sup> The key for initiating SWNT growth from fullerene cap is that the structure must be fully oxidized to open the carbon cage and activated by high-temperature annealing. Under certain thermal oxidation and annealing



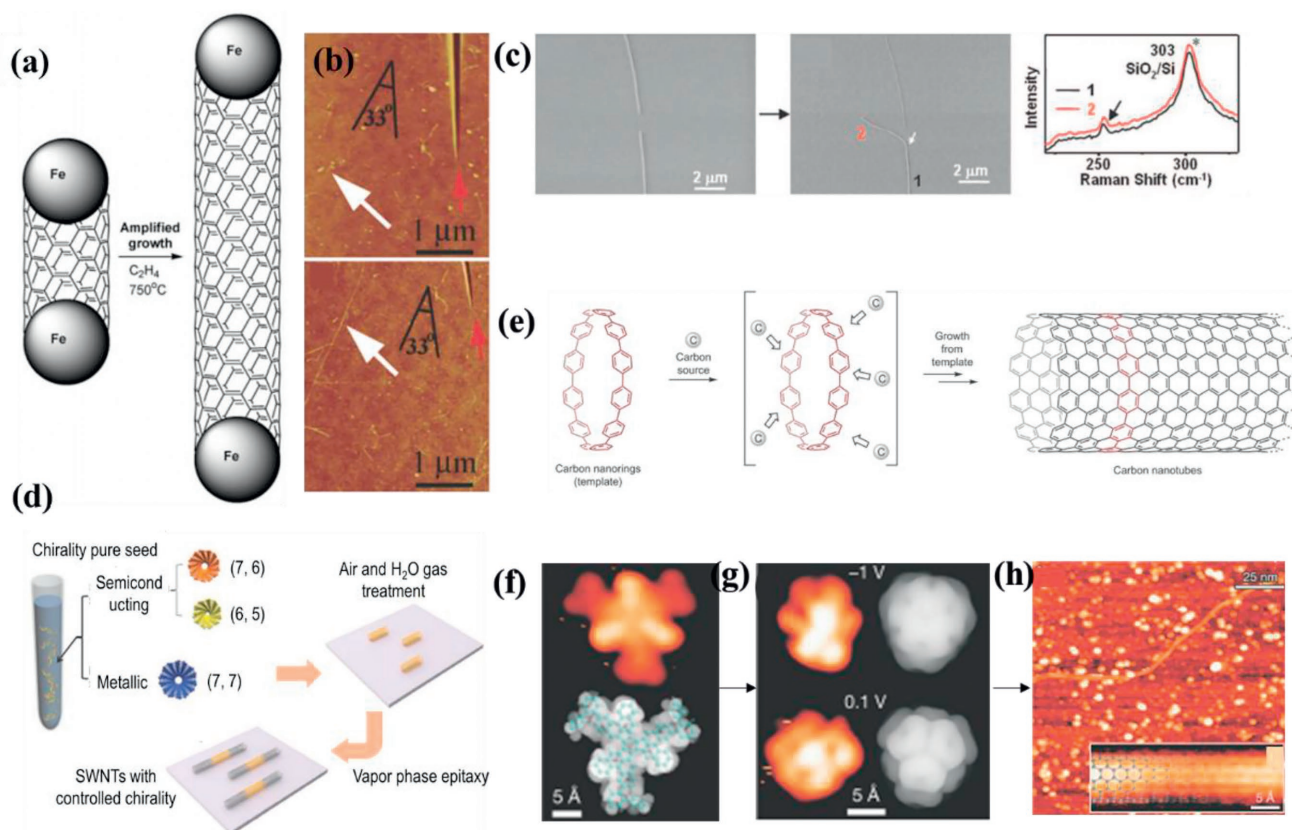


**Figure 10.** a) Schematic presentation of key steps for SWNT amplification. b) AFM images of the short SWNT “seed” and the amplified SWNT. a,b) Reproduced with permission.<sup>[128]</sup> Copyright 2006, American Chemical Society. c) SWNT “cloning” from “open ended” SWNT seeds and the Raman spectra of the SWNTs. Reproduced with permission.<sup>[130]</sup> Copyright 2009, American Chemical Society. d) Schematic illustration of the vapor-phase epitaxy process for chirality-controlled SWNT synthesis. Reproduced with permission.<sup>[131]</sup> Copyright 2012, Springer Nature. e) A general strategy for growing SWNTs from a carbon ring template. Reproduced with permission.<sup>[134]</sup> Copyright 2013, Springer Nature. Growth of (6, 6) SWNTs by bottom-up approach: f) the C<sub>96</sub>H<sub>54</sub> precursor; g) the SWNT seed; h) the synthesized long SWNT. f–h) Reproduced with permission.<sup>[37]</sup> Copyright 2014, Springer Nature.

conditions, only certain C–C bonds are selectively broken and form the carbon cages with limited possibilities, resulting in a step-like diameter distribution of SWNTs. Although the cap engineering using opened fullerene shows the potential to control SWNT chirality, the structure variation and coalescence of caps, constrains a precise control over the SWNT chirality.

Using a bottom-up strategy, Omachi et al.<sup>[134]</sup> proposed a programmable synthesis of structurally uniform SWNTs (Figure 10e). Cycloparaphenylenes carbon nanorings ([*n*] (CPP) where *n* represents the number of benzene rings) with controlled sizes, which represent the shortest sidewall segment of armchair SWNTs, are applied for growing carbon nanotubes. The template effect of the carbon ring is indicated by the diameter correlation between the [*n*] (CPP) and the resultant SWNTs, the diameters of synthesized SWNTs have a wide distribution. This work represents the first step toward the structurally uniform SWNTs by developing a truly programmable synthesis, showcasing the importance of the tremendous potential of organic chemistry approaches toward uniform SWNTs.

To avoid the imperfect fidelity in SWNT chirality control, Sanchez-Valencia et al.<sup>[37]</sup> prepared atomically precise ultrashort nanotube seeds which unambiguously dictate

the chiral index of formed SWNTs. The short capped (6, 6) seed is transformed from C<sub>96</sub>H<sub>54</sub> precursor monomer on Pt (1 1 1) surface (Figure 10f) through surface-catalyzed cyclo-dehydrogenation. The successful transformation is reflected by a prominent height increase from the originally quasi-planar three-fold symmetric molecules to dome-shaped species (Figure 10g). By epitaxial elongation, the surface anchored ultrashort caps evolve into targeted (6,6) SWNTs (Figure 10h). Instead of using metal particles, the findings illustrate the use of a planar metal substrate for producing a desired SWNT cap from a suitable precursor molecule, thus enables the highly selective SWNT synthesis. This method could provide SWNTs with identical electronic properties, solving one of the most pivotal challenges in realizing SWNT-based integrated circuits for digital electronics. However, further technologically relevant progress is required to improve the growth yield of SWNTs.

### 3.1.3. Synthesis of SWNTs by Template Catalysts

Different from the above template molecules, which generally suffer a high cost and low SWNT yield, catalyst nanoparticles

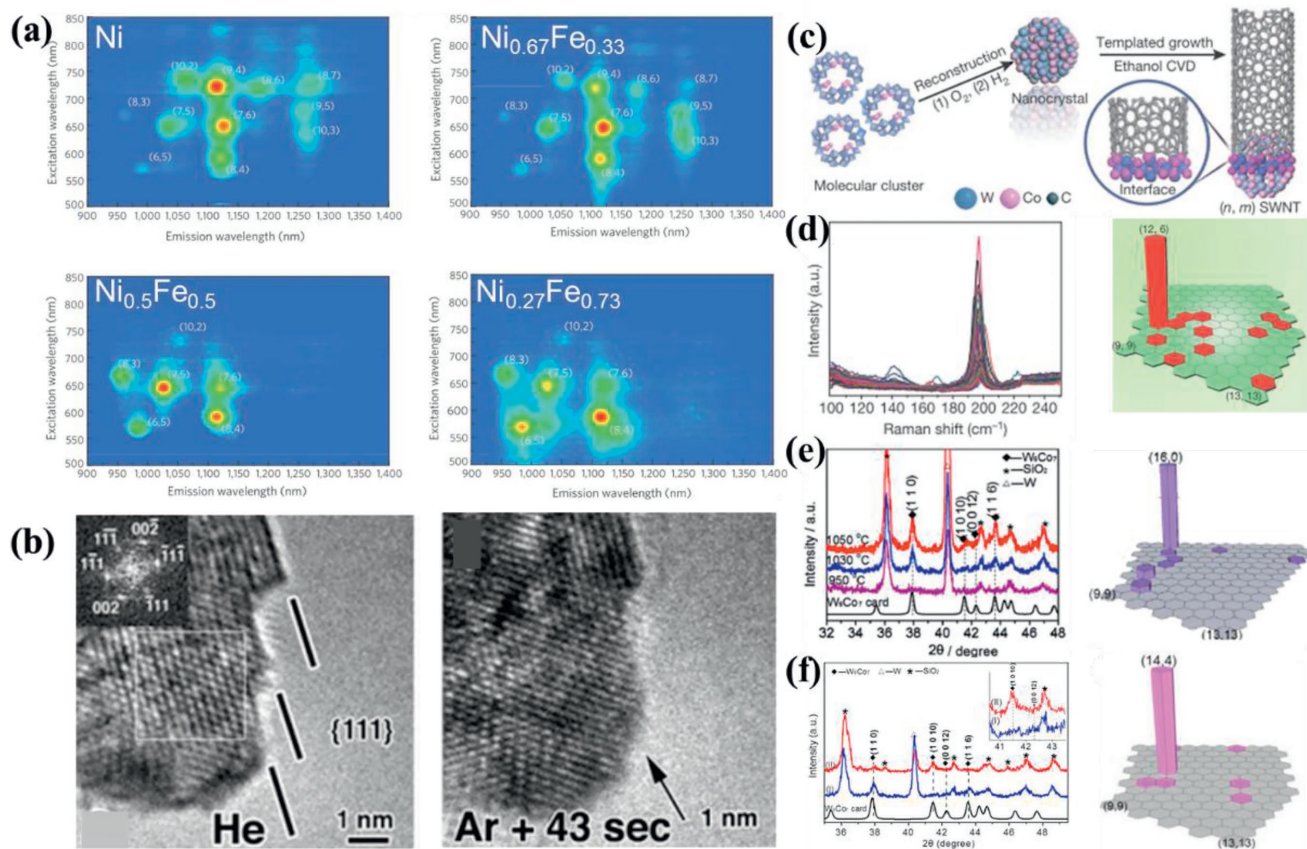


**Figure 11.** a) Contour plots of the PL as a function of excitation and emission for SWNT samples grown on different catalysts. Reproduced with permission.<sup>[99]</sup> Copyright 2009, Springer Nature. b) Morphology evolution of Fe nanoparticle in the presence of different gas atmosphere (He/H<sub>2</sub>O and Ar/H<sub>2</sub>O). Reproduced with permission.<sup>[30]</sup> Copyright 2009, American Association for the Advancement of Science. c) Schematic illustration of W–Co nanocrystal catalyst and the templated growth of an SWNT with specified (*n*, *m*). d) RBM region of Raman spectra for SWNTs synthesized by ethanol CVD on W<sub>6</sub>Co<sub>7</sub> alloy and the abundance of (12, 6) SWNTs. c,d) Reproduced with permission.<sup>[36]</sup> Copyright 2014, Springer Nature. e) XRD pattern of W<sub>6</sub>Co<sub>7</sub> alloy containing plenty of (1 1 6) planes and the chirality distribution of SWNTs grown on the catalyst. Reproduced with permission.<sup>[103]</sup> Copyright 2015, American Chemical Society. f) XRD pattern of W<sub>6</sub>Co<sub>7</sub> alloy with plenty of (1 1 10) planes, favoring the growth of (14, 4) SWNTs. Reproduced with permission.<sup>[104]</sup> Copyright 2016, American Chemical Society.

would allow a selective synthesis of SWNTs with low cost and high yield. When a certain (*n*, *m*) tube exactly matches the catalyst template and has the lowest formation energy, there is a possibility of selectively synthesizing this kind of SWNTs. For example, Chiang et al.<sup>[99]</sup> prepared a series of mono- and bimetallic Ni<sub>*x*</sub>Fe<sub>1-*x*</sub> nanoparticles with controlled Ni:Fe composition ratio for growing SWNTs at 600 °C. From the photoluminescence (PL) maps (Figure 11a), it is seen that the SWNT chirality distribution is correlated with the catalyst composition. Remarkably, the Ni<sub>0.27</sub>Fe<sub>0.73</sub> catalyst produces SWNTs with a much narrower chirality distribution and a singly dominating (8, 4) SWNT. The chirality distribution differences of SWNTs are attributed to the epitaxial growth of different SWNT caps on different solid catalyst. When Fe is incorporated into Ni lattice, the distance between atoms in the (1 1 1) plane increases. Such a compositional-tuning induced crystal structure perturbation affects the lattice match of the catalyst with certain chirality and leads to the observed shifts in the chirality distributions.<sup>[99]</sup> In support of the experimentally observed chirality selection on the catalysts, simulations performed by Dutta et al.<sup>[135]</sup> show

that (8, 4) SWNT cap is more stable on Ni<sub>0.27</sub>Fe<sub>0.73</sub> catalyst and (9, 4) SWNT cap is stable on pure Ni, accounting for the respective enrichments of SWNTs on the catalysts.

Although many previous reports claimed a possible match between SWNT structure and catalyst particles, direct experimental evidence on the structures of catalyst has been lacking. Using environmental TEM, Harutyunyan et al.<sup>[30]</sup> monitored the morphology variation of Fe nanoparticles in different gas environments during annealing process. A striking difference in the ripening behaviors relying on the gas environment is revealed. Very faceted Fe particle with sharp corners is observed in the presence of He/H<sub>2</sub>O (Figure 11b). The particle becomes more rounded when exposing to Ar/H<sub>2</sub>O ambient and is back to faceted shape upon returning to He/H<sub>2</sub>O. The observed dynamic alteration in the particle shape is caused by the surface energy anisotropy of specific facets of Fe, which is affected differently by the gas environment. Tuning the Fe nanoparticle morphology by varying gas ambient leads to the growth of metallic SWNTs with tunable population ranging from 18% to 91%. Particularly, the presence of H<sub>2</sub>O in catalyst

annealing supported by He promotes the growth of metallic SWNTs with dominant armchair ones. The armchair SWNT growth could be associated with the sharp morphology of Fe with (1 1 1) facets, facilitating the nucleation of armchair SWNTs with low formation energy. This work indicates a correlation between catalyst morphology and SWNT structure so that it is feasible to directly control the chirality of SWNTs by controlling catalyst structure.

In pursuit of growing SWNTs with a high single chirality purity, Li's group developed a novel  $W_6Co_7$  alloy catalyst for the selective synthesis of SWNTs with specific  $(n, m)$  (Figure 11c).<sup>[36]</sup> Owing to the alloying with W, the  $W_6Co_7$  alloy catalyst has a high melting temperature and is able to preserve its crystal structure during the CVD process. Meanwhile, the presence of Co in the catalyst guarantees a high SWNT growth efficiency. The Raman spectra of SWNTs grown by ethanol CVD at 1030 °C show a prominent radial breathing mode (RBM) peak centered at  $\approx 197\text{ cm}^{-1}$ , assigned as (12, 6) SWNT (Figure 11d). Based on the Raman characterizations on  $\approx 3300$  detected RBMs and counting for the coverage of excitation, the abundance of (12, 6) SWNT is estimated to be 94.4% (Figure 11d), in agreement with that calculated from the UV-vis-NIR absorption spectrum. The results demonstrate that it is possible to directly synthesize SWNTs with a dominant single chirality. DFT calculations were performed to fit different SWNTs to the (0 0 12) plane of a  $W_6Co_7$  alloy. A perfect geometrical match between (12, 6) SWNT and  $W_6Co_7$  (0 0 12) plane is revealed. In contrast, SWNTs with other chiralities have poor matches with the plane. In addition, the low arrangement uniformity of Co in the alloy nanoparticle enhances a more specific structural match between (12, 6) SWNT and the catalyst.<sup>[36]</sup> Such a perfect structural match between catalyst and SWNT is an essential factor in the chirality-specific growth. This work presents the thermodynamic ascendancy for chirality-selective growth of SWNTs.

The structural match restricts the nucleation and growth of SWNTs with specific  $(n, m)$ . Li et al.<sup>[103]</sup> further applied the same  $W_6Co_7$  alloy which contains plenty of (1 1 6) planes for CVD synthesis of zigzag (16, 0) SWNTs. X-ray diffraction pattern of the catalyst exhibits an extremely strong (1 1 6) peak (appearing at  $43.6^\circ$ ), indicating the population of (1 1 6) planes (Figure 11e). DFT calculations choose the catalyst structure cutting from the (1 1 6) plane to study the structural match of SWNTs with different chiralities. As indicated by the interface energy, templated growth of (16, 0) SWNT could be initiated on (1 1 6) plane of  $W_6Co_7$  catalyst. Indeed, under optimal ethanol CVD conditions, selective growth of (16, 0) SWNTs with a purity of 80% is achieved on the (1 1 6) planes of  $W_6Co_7$  catalyst. However, owing to the perfect structural match between SWNT and the surface of the alloy catalyst, the growth rate of (16, 0) SWNT is very low as it is difficult to destroy the perfect contact between SWNT and catalyst. The results indicate an unfavorable growth kinetics of zigzag (16,0) SWNTs because of the lack of kinks at the tube-catalyst interface. This work further highlights the advantages of using catalyst surface as the template for synthesizing SWNTs with low formation energy. Similarly, (14, 4) SWNTs with a purity as high as 97% was successfully synthesized on the (1 0 10) planes of  $W_6Co_7$  catalyst (Figure 11f), which had been pretreated with  $H_2O$  to

regulate the structure.<sup>[104]</sup> The  $H_2O$  treatment modifies the catalyst surface energy and leads to the enrichment of (1 0 10) planes. DFT simulations show that the circumstance of a (14, 4) SWNT well matches the atomic arrangements in (1 0 10) plane. All carbon atoms are reasonably bonded with the metallic atoms in (1 0 10) plane of the catalyst without any deformation of the cylinder configuration. Therefore, the (1 0 10) plane could act as a template for the preferential nucleation and growth of (14, 4) SWNTs.

Besides W-Co alloy nanocatalyst, other W-based alloy, such as W-Fe and W-Ni were also proved to be efficient in selectively growing SWNTs with certain chirality.<sup>[36]</sup> The series of work not only offers a possible solution for selectively growing  $(n, m)$  SWNTs by employing high-melting-temperature alloy catalyst, but also opens a new avenue for growing SWNTs with high chirality selectivity via perfectly matching the structure of template catalyst.

### 3.2. Chirality Selection by Combining Thermodynamic Control and Kinetics Control

#### 3.2.1. Catalytic Synthesis of One-Index-Off SWNTs

Multiplying both the nucleation (thermodynamics factor) and growth term (kinetic factor) presents the population of SWNTs with certain chirality (Figure 9a). At low reaction temperature, if armchair SWNTs have the lowest tube-catalyst interface energies but negligible growth rate, a predominance of  $(n, n - 1)$  near-armchair SWNTs with a single kink can be expected. One key to achieve such enrichment is to design catalysts in which the active component is preserved in solid state during CVD synthesis. Most nanocatalysts, consisting of active components such as Fe, Co, or Ni do not have a higher melting temperature. Therefore, a low CVD temperature is demanded to achieve a high chirality selection. The first reported catalyst for selectively generating (6, 5) SWNTs is CoMoCAT,<sup>[31]</sup> where the CVD growth is performed at about 700 °C.<sup>[50]</sup> The catalyst is effective only when both Co and Mo are simultaneously present, suggesting a synergistic effect between Co and Mo is essential for the performance of the catalyst (Figure 12a).<sup>[66,136]</sup> The chirality distribution of SWNTs is extensively investigated by optical techniques.<sup>[31,137,138]</sup> Remarkably, with resonance Raman scattering, Jorio et al.<sup>[138]</sup> quantify the amount of each SWNT species (Figure 12b), giving an estimated (6, 5) SWNT abundance of 40%. The preferential synthesis of (6, 5) SWNTs emerges from the two antagonistic trends at the catalyst-tube interface: energetic preference toward achiral versus the faster growth kinetics of chiral ones, as addressed by Artyukhov et al.<sup>[83]</sup>

By designing a USY-zeolite supported FeCo catalyst, near-armchair SWNTs were preferentially grown from alcohol CVD.<sup>[32,91]</sup> Figure 12c is a PL map of SWNTs synthesized at 650 °C, only two dominant emission peaks corresponding to SWNTs with chiral indices (6, 5) and (7, 5) are observed. The state of the active components (Fe and Co) in the catalyst is supposed to be solid at so low a temperature, guiding nucleation and elongation of near-armchair species. Selective growth of (6, 5) SWNTs is also achieved by methane CVD at 600 °C on



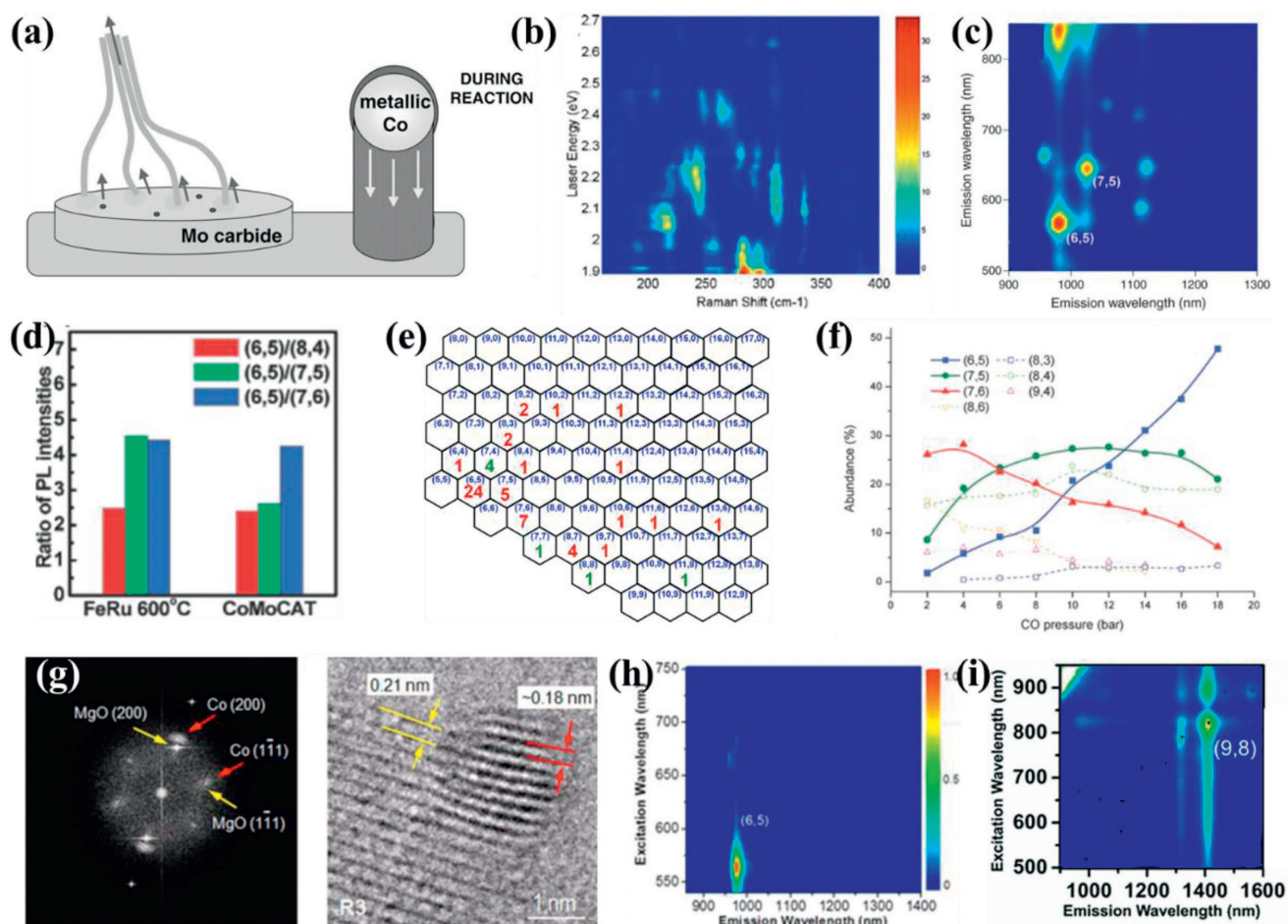


**Figure 12.** a) Schematic representation of Mo stabilized Co for growing SWNTs. Reproduced with permission.<sup>[66]</sup> Copyright 2006, American Scientific Publishers. b) RBM spectra against laser energy for as-produced CoMoCAT SWNT samples. Reproduced with permission.<sup>[138]</sup> Copyright 2005, American Physical Society. c) Contour plots of fluorescence spectra as a function of excitation wavelength for SWNTs grown on zeolite-supported FeCo catalyst by alcohol CVD. Reproduced with permission.<sup>[91]</sup> Copyright 2004, Elsevier B.V. d) PL intensity ratios between the (6, 5) SWNT and the (8, 4), (7, 5), and (7, 6) tubes in 600 °C grown FeRu tubes versus CoMoCAT tubes. Reproduced with permission.<sup>[33]</sup> Copyright 2007, American Chemical Society. e) Chirality map of SWNTs grown on FeCu/MgO catalyst at 600 °C. Reproduced with permission.<sup>[92]</sup> Copyright 2012, American Chemical Society. f) The abundance of different  $(n, m)$  SWNT evolution with CO pressure. Reproduced with permission.<sup>[144]</sup> Copyright 2007, American Chemical Society. g) Fast Fourier transform pattern of reduced Co on MgO support, showing the epitaxial relationship between Co and MgO. High-resolution TEM image demonstrates a lattice mismatch epitaxy. h) PL contour plot of the SWNTs grown at 500 °C on the  $\text{Co}_x\text{Mg}_{1-x}\text{O}$  solid solution. g,h) Reproduced with permission.<sup>[59]</sup> Copyright 2013, Springer Nature. i) PL contour plot of SWNTs grown on Co-TUD catalyst by pressured CO CVD. Reproduced with permission.<sup>[101]</sup> Copyright 2010, American Chemical Society.

a silica-supported FeRu catalyst.<sup>[33]</sup> In the PL map, (6, 5) tube exhibits the most intense emission intensity and other SWNT species have very weak signals. The relative concentration of (6, 5) tube is evaluated by analyzing the  $(6, 5)/(n, m)$  [for  $(n, m) = (7, 6), (7, 5),$  and  $(8, 4)$ , respectively] PL intensity ratios (Figure 12d). Compared with CoMoCAT SWNTs, the FeRu grown SWNTs are similarly enriched in the (6, 5) SWNT relative to other  $(n, m)$  tubes. Although there are no detailed characterizations on the catalyst, solid Fe nanoparticles are supposed to be the templates for promoting (6, 5) SWNT synthesis.

A higher chirality selectivity toward (6, 5) SWNT is obtained on a MgO-supported FeCu catalyst.<sup>[34,92]</sup> Using CO CVD at a reaction temperature of 600 °C, high quality SWNTs are produced on the FeCu catalyst. The growth of SWNTs from FeCu catalyst at 600 °C is attributed to the synergistic effect: under the reaction environment, the CuO could be easily

reduced and adsorb reductive species, which can “spillover” to the adjacent iron oxide, facilitating the reduction of iron oxide, leading to the subsequent growth of SWNTs.<sup>[34]</sup> Such a postulation is well confirmed by in situ environmental TEM characterizations,<sup>[92]</sup> demonstrating the easy reduction of CuO at low temperatures and the SWNT growth on Fe nanoparticles. PL and nanobeam electron diffraction characterizations on 600 °C-grown SWNTs reveal a predominant synthesis of (6, 5) SWNTs (Figure 12e).

The low reaction temperature during CVD process guarantees the solid state of the catalyst particle, which is essential for chirality-selective synthesis of SWNTs. Precisely, it is the morphology and the related exposed facets of the solid catalyst that encode the nucleation and elongation of SWNTs, accounting for the chirality distributions of synthesized SWNTs. Among the catalysts that are applicable for low

temperature synthesis of SWNTs, including FeRu,<sup>[33]</sup> FeCo,<sup>[91]</sup> CoPt,<sup>[94]</sup> CoCu,<sup>[139]</sup> CoMn,<sup>[93]</sup> FeMn,<sup>[97]</sup> Co,<sup>[51,140,141]</sup> Ni,<sup>[96,99,142]</sup> Fe,<sup>[97,143]</sup> and Au,<sup>[95]</sup> Fe-based catalysts afford the most enriched (6, 5) species under similar growth conditions. The phenomena could be explained by the low (6, 5) SWNT-Fe interfacial energy, favoring the nucleation and subsequent growth of (6, 5) SWNTs.

With increasing reaction temperature, most major species synthesized on the above catalysts do not centered at  $(n, n - 1)$  SWNTs anymore. For products synthesized on FeCu catalyst at over 800 °C, intense PL emission intensities are observed for (7, 5) and (8, 4) SWNTs.<sup>[34]</sup> Similar enrichment of the two SWNT species are also reported on FeRu catalyst synthesized at 850 °C.<sup>[33]</sup> At such a high reaction temperature, the catalyst nanoparticle could be in liquid state, mitigating the map formation energy differences and decrease the selectivity to  $(n, n - 1)$  species.<sup>[83]</sup> Under this circumstance, SWNT growth kinetics might prevail in determining the chirality distributions. Consequently, to promote the growth of near-armchair SWNTs at high reaction temperature, strategies which can increase the melting temperature of active component, such as increasing metal-support interactions and enhancing the reaction pressure, could be applicable.

Indeed, when applying high pressures during CVD, Co-based catalysts are also capable of growing SWNTs with dominant (6, 5) species using CO as the carbon source.<sup>[93,144]</sup> For example, Zoican Loebick et al.<sup>[93]</sup> reported a CoMn-MCM-41 catalyst for high pressure synthesis of (6, 5) SWNTs. Such an enrichment on Co-based catalyst is coherently related to the high CO pressure applied during SWNT synthesis process. To study the pressure effect, Wang et al.<sup>[144]</sup> plotted the chirality distribution of SWNTs against reaction pressure (Figure 12f). At a reaction pressure of 2 bar, the total abundance of  $(n, n - 1)$  SWNTs is about 28%. The  $(n, n - 1)$  SWNT abundance increases with the reaction pressure and reaches 55% in the product grown at 18 bar. The results indicate that high pressure facilitates the enrichment of  $(n, n - 1)$  SWNTs. The high CO pressure, on the one hand, can increase the melting temperature of reduced Co nanoparticles, which can be preserved as a solid template for SWNT growth. On the other hand, the high CO pressure induces a Co nanoparticle morphology change compared to Co particle at a low CO pressure. Such a morphology change would result in nanocrystals with certain concentrated planes, promoting the nucleation of (6, 5) SWNTs.

The morphology regulation of Co nanocrystal can also be realized by exerting an external stress at the metal-support interface.<sup>[59]</sup> A  $\text{Co}_x\text{Mg}_{1-x}\text{O}$  solid solution which affords the epitaxial formation of Co nanoparticles upon reduction was designed for chiral selective growth of SWNTs.<sup>[59]</sup> Upon reduction, homogeneous crystalline Co nanoparticles having an epitaxial relationship with the MgO support migrate onto the surface (Figure 12g). Due to an unusually large mismatch in their lattice constant, the Co nanocrystal is severely strained to accommodate the lattice of the MgO matrix with unique morphology. During SWNT nucleation and elongation, the crystalline Co nanoparticles preserve their crystalline orientations and demonstrate little structural fluctuation, producing SWNTs with predominant (6, 5) species (Figure 12h).<sup>[59]</sup> The results demonstrate that the epitaxially formed Co nanoparticles

promote highly chiral-selective growth of SWNTs. This work thus provides an efficient approach for regulating the chirality distribution of SWNTs nucleated on the catalyst.

To successfully grow enriched (6, 5) SWNTs, the size of nanoparticles should be kept small enough using some anchors. In the previously reported catalysts systems, the metal nanoparticles can be anchored by either the substrate or a second metal to constrain the aggregation of reduced metal particles. In the bimetallic catalysts, such as CoMo,<sup>[31]</sup> FeCu,<sup>[34]</sup> FeRu,<sup>[33]</sup> and FeMn,<sup>[97]</sup> the anchoring agents are Mo, Cu, Ru, and Mn, respectively. In the case of monometallic catalysts,<sup>[51,96,142,145]</sup> the unreduced metal ions are supposed to have strong interactions with the metallic counterparts, preventing the coalescence of reduced species. In the case of MgO-supported Ni catalyst,<sup>[142]</sup> DFT calculations model the binding energy between Ni(0) on a MgO slab, which reveals that the binding energy increases when increasing the number of substituted  $\text{Ni}^{2+}$ . The results demonstrate that the substituted  $\text{Ni}^{2+}$  can act as an anchor site to stabilize the reduced Ni. This work highlights the importance of anchoring effect in stabilizing small diameter particles for selectively growing (6, 5) SWNT.

As there is correlation between catalyst size and tube diameter, to explore the preferential synthesis of  $(n, n - 1)$  SWNTs with relatively large diameters, solid nanocatalyst with large diameters are required during CVD process. Aiming at this goal, Wang et al.<sup>[101]</sup> developed a Co incorporated TUD-1 catalyst for selectively growing (9, 8) SWNTs. Under optimal reduction and growth conditions, (9, 8) SWNT with a population of 59.1% is achieved (Figure 12i). It is revealed that the prerduction temperature plays a critical role in determining the (9, 8) SWNT selectivity. The optimal reduction temperature of 500 °C is correlated with the catalyst reduction temperature (483 °C) and facilitates the formation of 1.2 nm Co nanoparticles. Varying the reaction temperature in the range of 600–800 °C only affect SWNT yield rather than chirality distribution, indicating that the reduced Co nanoparticles could preserve a solid state and suitable diameters, guiding the nucleation and growth of (9, 8) SWNTs.

Subsequently, a sulfur-promoted  $\text{CoSO}_4/\text{SiO}_2$  catalyst was also developed for selective synthesis of (9, 8) tubes.<sup>[146]</sup> In its  $\text{H}_2$  temperature programmed reduction profile, the catalyst exhibits a narrow reduction peak centered at 470 °C. The narrow reduction window leads to the formation of Co particles with a narrow diameter distribution. In addition, the coexistence of sulfur atom near Co inhibits the coalescence of reduced Co nanoparticles, which is determined to have an average size of 1.23 nm by X-ray absorption spectroscopy. The narrow diameter distribution of Co nanoparticles leads to the selective synthesis of (9, 8) SWNTs. Alternatively, the selective growth of (9, 8) SWNTs could also be realized by introducing sulfur-containing compounds, such as disulfide and thiophene into carbon feedstock during CVD process.<sup>[147]</sup> When the sulfur concentration in ethanol exceeds a threshold value, the sulfur might selectively block active sites on Co particles through dynamic interactions among sulfur, hydrogen, carbon and Co particles, accounting for the (9, 8) chirality selection. However, like many other high-chirality-selectivity SWNT growth,<sup>[35]</sup> the (9, 8) SWNT chirality selection comes with compromises in the SWNT yield.

To improve SWNT chirality selectivity while maintaining carbon yield, Yuan et al.<sup>[102]</sup> proposed a “smart poisoning” of Co/SiO<sub>2</sub> catalyst for (9, 8) SWNT synthesis by sulfidation using a mixture of H<sub>2</sub>S and H<sub>2</sub>. Such a sulfidation process triggers the formation of structurally controlled Co<sub>9</sub>S<sub>8</sub> species, serving as an intermediary compound and assisting the generation of metallic Co nanoparticles with a narrow diameter distribution upon reduction. The reduced Co nanoparticles ultimately result in the chirality-selective growth of SWNTs around (9, 8) species. More importantly, different from previous catalysts in growing chirality-selective SWNTs, the sulfidation of Co/SiO<sub>2</sub> does not decrease its activity while enhancing the (9, 8) SWNT selectivity. The carbon yield of sulfide catalyst is around 2.5%, close to that of Co/SiO<sub>2</sub> catalyst (2.7%). This approach would lead to the mass production of highly active catalysts for large production of chirality-defined SWNTs without sacrificing the carbon yield.

To obtain (*n*, *n* - 1) SWNTs with much larger diameters, such as (13, 12) and (12, 11), Zhu et al.<sup>[100]</sup> reported a NH<sub>3</sub> promoted synthesis of such near armchair SWNTs by floating ferrocene CVD. During the floating CVD process, the Fe nanoparticles are generated in situ for catalyzing the growth of SWNTs. The Fe particles deriving from ferrocene vapor decomposition have relatively large diameters,<sup>[148]</sup> and could be in solid state in the reaction environment (880 °C). In the products synthesized with the addition of NH<sub>3</sub>, near armchair SWNTs, including (13, 12), (12, 11), and (13, 11) constitute nearly 30%

of the investigated SWNTs. The average diameter of SWNTs is 1.67 nm and over 90% distribute in the high chiral angle region (20°–30°). During the growth, the presence of NH<sub>3</sub> would favor the formation of solid Fe nanoparticles with specific enriched planes, leading to the enrichment of near armchair (*n*, *n* - 1) SWNTs. The SWNT diameter is constrained by the size of catalyst particle, which affords SWNT growth by perpendicular mode, limiting the growth of SWNTs in a slice of the map centered at (13, 12) and (12, 11).

### 3.2.2. Catalytic Synthesis of SWNTs from Symmetry Match

By similar logic, it is possible to synthesize other specific (*n*, *m*) SWNT which matches the catalyst template, especially when the SWNT also has a high growth rate. The fast-growing tubes have a magic chiral angle of 19.1°, corresponding to (2*m*, *m*) SWNTs.<sup>[83]</sup> Although previous work of Yang et al.<sup>[36]</sup> reported the preferential growth of (12, 6) SWNT, the SWNT growth kinetics had not been investigated. Zhang et al.<sup>[38]</sup> recently performed controlled experiment to investigate the growth kinetics of SWNTs on solid catalysts and proposed a rational strategy for growing (2*m*, *m*) SWNTs (Figure 13a). In order to confirm the role of kinetic control, the ratio of C/H (ethanol: H<sub>2</sub> = 100/200) abruptly increases after 5 min of growth to 100/0. Optical characterizations show that (2*m*, *m*) tubes with chiral angle of 19.1° are the longest among all the detected

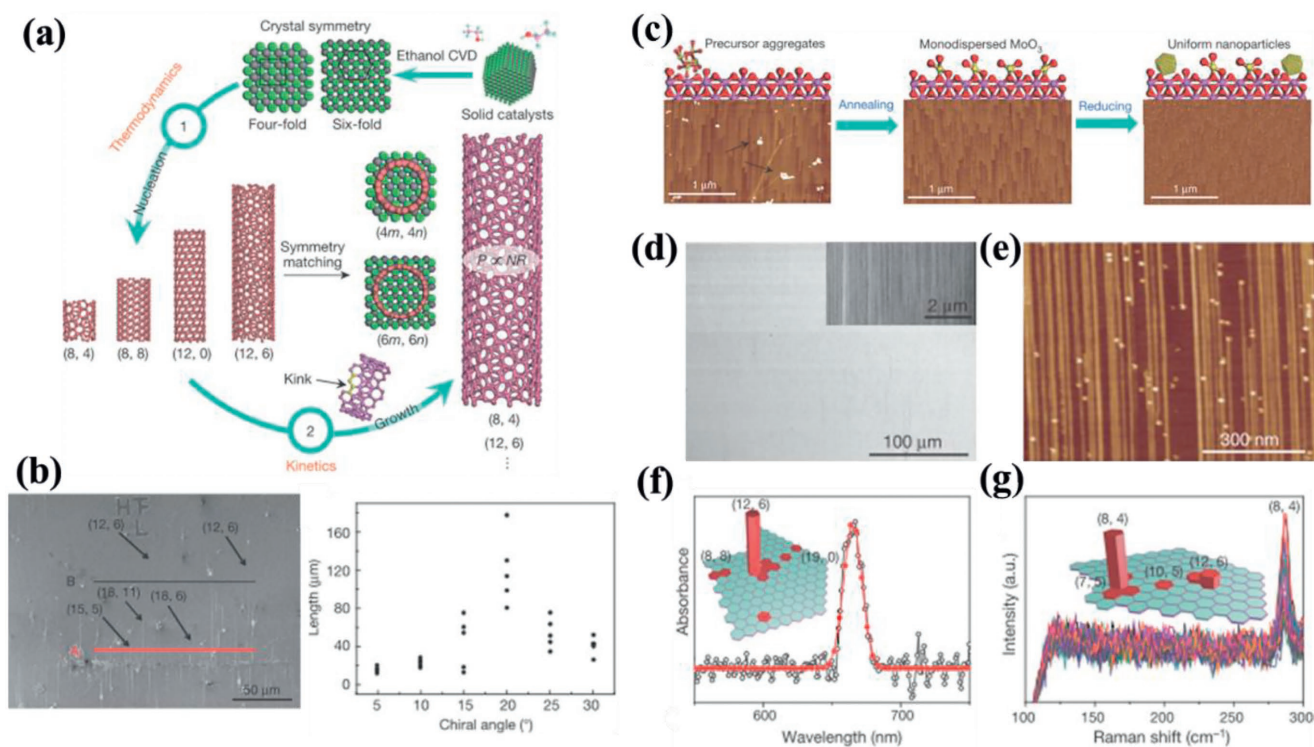


**Figure 13.** a) Control of the SWNT chirality by combining thermodynamic and kinetic control from ethanol CVD. b) SEM images of SWNTs grown by abrupt carbon feedstock increase. The lengths of SWNT plots against their chiral angles determined by optical techniques. c) The strategy for preparing uniform Mo<sub>2</sub>C nanoparticles. d) SEM and e) AFM images of SWNTs grown on Mo<sub>2</sub>C. f) Absorption spectrum of SWNTs grown on Mo<sub>2</sub>C, showing a preferential synthesis of (12, 6) SWNT. g) Raman spectra of SWNTs grown on WC, demonstrating an enrichment of (8, 4) SWNT. Reproduced with permission.<sup>[38]</sup> Copyright 2017, Springer Nature.



SWNTs, confirming the  $(2m, m)$  tubes have the highest growth rate and are kinetically favored because of the most kinks at tube edges available for carbon incorporation (Figure 13b). SWNTs nucleated on catalyst without many kinks could be easily deactivated by excessive carbon supply, greatly promoting the chirality selectivity of  $(2m, m)$  SWNTs with the most kinks. As a result, with the increase of C/H ratio, SWNTs with chiral angles other than  $19.1^\circ$  and less kinks could be deactivated, enhancing  $(2m, m)$  SWNT chirality selectivity.

When considering the thermodynamically stable existence of SWNTs, a symmetry match should be taken into account. A low formation energy and a high population is expected if the SWNT symmetry matches that of solid catalyst. For example, a  $\text{Mo}_2\text{C}$  (0 0 1) plane with near six-fold symmetry matches the 6-fold symmetry of (12, 6) SWNTs,<sup>[38]</sup> which are calculated to have a low formation energy. This is because the carbon atoms on the open end of SWNTs can properly anchored to the catalyst surface with the same symmetry and binds much stronger to the catalyst surface than SWNTs with different symmetries. In fact, previous growth of (12, 6) SWNTs on (0 0 12) planes of  $\text{Co}_6\text{W}_7$  also has such a symmetry match between the SWNT and the catalyst plane.<sup>[36]</sup> However, it is noted that the formation energy of (12, 6) SWNT is not the global minima of the energy landscape. For example, armchair (12, 12) tubes could possess the lowest formation energy of catalyst surface because they also have the same 6-fold symmetry and perfectly matches the catalyst surface. However, when taking the growth kinetics into account, the energy barrier for incorporating carbon atoms to the open edges of armchair SWNTs is extremely high,<sup>[83]</sup> excluding the enrichment of armchair species in a reasonable abundance.

Besides controlling SWNT growth thermodynamics and kinetics, a constrain on catalyst diameter is a key prerequisite for achieving certain  $(n, m)$  SWNT with a high population. A strategy proposed by Zhang et al.<sup>[38]</sup> is proven to be successful in forming uniformly sized Mo nanoparticles on sapphire surface (Figure 13c). In the approach, a monolayer  $\text{MoO}_3$  first forms on sapphire surface by the generation of Mo-O-Al bonds under annealing. Excessive  $\text{MoO}_3$  vaporizes because of its high volatility. Upon reduction, uniform Mo particle appears on the sapphire surface and are readily transformed into  $\text{Mo}_2\text{C}$  once introducing carbon precursor at high temperatures. Using the uniform  $\text{Mo}_2\text{C}$  nanocrystal as the catalyst, SWNTs with a narrow chirality distribution is synthesized by ethanol CVD. Figure 13d presents an scanning electron microscopy (SEM) image of the carbon nanotubes grown on sapphire substrate. Horizontally well-aligned carbon nanotubes with a density of  $\approx 20$  tubes  $\mu\text{m}^{-1}$  are observed. AFM characterizations further demonstrate that a highest density with 40 tubes  $\mu\text{m}^{-1}$  can be achieved on sapphire (Figure 13e). Height section statistics shows that the SWNTs have a very narrow diameter distribution and a mean diameter of 1.21 nm, which is close to the diameter of the (12, 6) nanotube (1.24 nm). Based on the results of different optical characterization techniques, the abundance of (12, 6) SWNT is estimated to be  $\approx 90\%$  (Figure 13f). Therefore, an enrichment of (12, 6) SWNT is achieved on  $\text{Mo}_2\text{C}$  with a six-fold symmetry. Similarly, horizontally aligned semiconducting (8, 4) SWNTs with an abundance of over 80% is preferentially synthesized on uniformly sized WC with a four-fold symmetry.

Thermodynamically, symmetry matching leads to the nucleation of nanotubes with four-fold symmetry, such as (8, 4), (12, 4), (12, 8), and (16, 8) tubes. Among these tube species, only  $(2m, m)$  SWNTs, such as (8, 4) and (16, 8) tubes with the most kinks are kinetically favored. Further constrain the SWNT diameter distribution by applying WC nanoparticles with mean size of 1.08 nm, predominant synthesis of (8, 4) SWNTs with a density of 10 tubes  $\mu\text{m}^{-1}$  and a selectivity of 80% is achieved (Figure 13g). The high-density aligned semiconducting SWNTs are readily applied for future nanoelectronics devices. The findings highlight the importance of symmetry matching between catalysts and nanotubes for controlling SWNT nucleation, which could ultimately guide the growth of SWNTs with predicted chirality.

#### 4. Conclusions and Prospects

The growth mechanisms of SWNTs in catalytic CVD is very complicated because of the various reaction parameters involved, such as the catalyst, support, carbon source, reaction temperature, and pressure. The catalyst–support interaction governs whether the SWNT growth follows a tip-growth mode or base-growth mode. The growing SWNT takes either VLS or VSS mechanism depending on the physical state of the catalyst. The growth mode (tangential or perpendicular) dictates the diameter ratio between SWNT and catalyst particle. Despite of the complex mechanism, simplified models have been developed to describe the origins of SWNT chirality selection, where the SWNT–catalyst interface plays essential roles: thermodynamic preference to lower energy nucleus and kinetic preference of higher growth rate. As the flat energy landscape of SWNT end-caps reveals no chiral angle bias for their nucleation, the contact energies at SWNT–catalyst interface control the nucleation probability of  $(n, m)$  SWNT. Compared with liquid catalyst, which favors the nucleation of SWNTs with low interfacial formation energy and shows little dependence on the catalyst features, solid catalysts, which could possess different morphology and exposed facets, have shown great potential in regulating the nucleation of SWNTs with specific  $(n, m)$ . The solid catalyst can be short SWNTs, opened fullerene caps, or predefined molecular seeds, which have been amplified into long SWNTs. W-based alloy nanoparticles, preserving the solid state at high reaction temperature, afford the nucleation and growth of SWNTs structurally matching the underlying catalyst facet. Such a tube–catalyst structural match facilitates the nucleation of SWNTs having a low formation energy on the catalyst. The dominant SWNT chirality differs when changing the relative abundances of different crystal facets. Kinetically, SWNTs with tight contact on solid catalyst might have very low growth rate. One-index-off SWNT is enriched to allow for rapid kinetics at the cost of higher energy of the nucleation. This is the case for bulk growth of SWNTs on transition metals at low reaction temperatures. By tuning the size of the catalyst particles,  $(n, n - 1)$  SWNTs with controlled diameters and chiralities are synthesized. Together with thermodynamic and kinetic control, constraints on the diameters from catalyst size lead to the predominance of  $(2m, m)$  SWNTs with fastest growth rates. The SWNT species which have been enriched during growth are

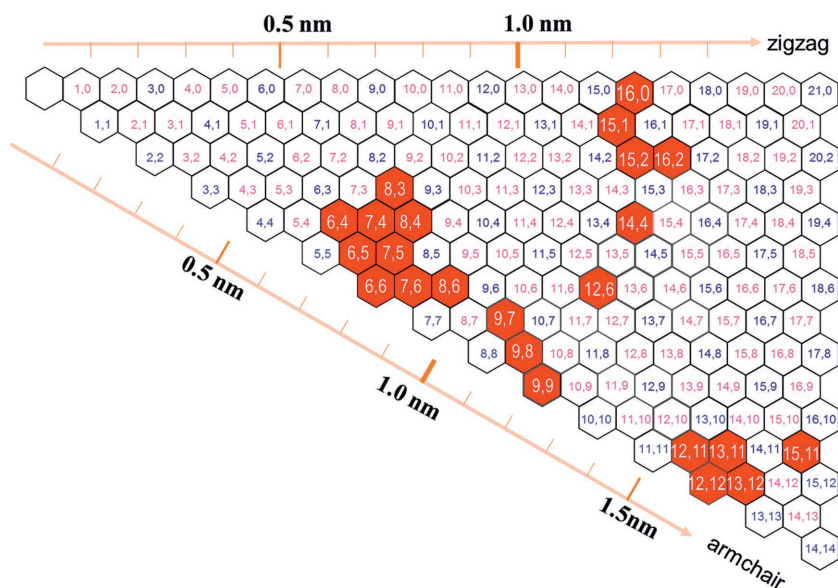


**Figure 14.**  $(n, m)$  SWNT species (red hexagon) achieved so far by direct chirality selection synthesis.

indicated in the **Figure 14**. In some cases, the single chirality even reaches over 90%.<sup>[36,38,104]</sup>

However, to meet the demand of high performance nanoelectronics, single chirality SWNTs with a purity higher than 99.999% is necessary.<sup>[17]</sup> Consequently, it is still an urgent task to greatly improve the selectivity of SWNTs with defined chirality. Grounded on the previous achievements, the following issues should be considered for enriching SWNTs with single chirality and ultra-high purity: (i) To gain more insights in the SWNT nucleation and growth mechanisms. In situ techniques, like in situ Raman spectroscopy and environmental TEM have provided valuable information regarding SWNT growth kinetics and thermodynamics. Although many efforts have been dedicated to catalyst evolution,<sup>[74,149]</sup> tube nucleation,<sup>[59,71]</sup> tube elongation<sup>[92,150]</sup> and growth termination,<sup>[151]</sup> SWNT chirality information acquired during in situ growth remains limited. The fragmentary evidences and the resolution limitations prevent the establishment of a complete view for SWNT growth. Simulations arise as a complement for addressing the origin for SWNT chirality selection. However, such calculations are performed at an ideal circumstance and the practical SWNT growth environments are far different. Therefore, to validate the previously proposed models and Figure out more central issues for chirality control, more controlled ex situ/in situ experiments should be carefully performed. Recent experimental results demonstrate that metal particles are negatively charged due to the occurrence of an electrochemical process in the surface reaction step.<sup>[152]</sup> The presence of charge would definitely affect the tube-metal interfacial energy, having significant impact on the chirality of produced SWNT. Consequently, synthesis of SWNTs with controlled conductivity or chirality is expected by taking advantage of the charge characters of catalysts in the future. (ii) To improve the yield of SWNT cloning. The advantage of cloning, especially for SWNT segments, is that the elongated parts would inherit the structures of their parent tubes. Although this approach provides a means

of designing and synthesizing any desired  $(n, m)$  SWNT, the cloning efficiency is not high,<sup>[130]</sup> limiting the scale up of the process. Strategies, which would increase the cloning efficiency and promote the formation of other SWNT chirality from molecular seed,<sup>[153]</sup> would shed more light on chirality-controlled synthesis of SWNTs. (iii) To design novel catalyst templates for SWNTs with other chirality. So far, the highest chirality selectivity is mainly achieved by symmetry match for surface-grown (12, 6) with six-fold symmetry and (8, 4) SWNTs with four-fold symmetry.<sup>[36,38]</sup> SWNTs with other symmetries are rarely synthesized selectively. In the chiral map, the portion of SWNTs with  $p$  symmetry is proportional to  $1/p^2$ . The larger the  $p$  value is, the easier to control the synthesis of SWNTs. For example, for SWNTs with five-fold symmetry, the smallest chiral SWNTs is (10, 5) tube, which could be selectively grown when applying catalysts with active planes of fivefold symmetry, such as quasicrystal or

twinned nanoparticles. Together with controlling SWNT diameters by tuning catalyst size, direct CVD synthesis of single chirality SWNTs with a high purity is expected. (iv) To control the SWNT growth mode. This is a precondition for controlling SWNT diameter and chirality. The key factor that determines SWNT growth mode for catalysts in different physical state should be clarified to guide a ration control. (v) To regulate the growth termination of SWNTs for improving chirality selection. Although perfect match between the  $(n, m)$  SWNT and the catalyst favors the nucleating of the SWNT because of the low formation energy, SWNTs with one index off, including  $(n - 1, m)$  and  $(n, m - 1)$  might also tend to nucleate with nonnegligible concentrations, challenging the selective synthesis of single chirality SWNT with ultra-high purity. Overfeeding carbon to catalyst is proposed to be an efficient route to survive catalysts nucleating SWNTs with more kinks. With intentional overfeeding of carbon, catalysts inducing SWNTs with less kinks and consuming less carbon atoms during growth will be deactivated because of the possible encapsulation by precipitated carbon layer. Using such a strategy, the selectivity of SWNTs with one specific chirality would be greatly enhanced. (vi) Bulk synthesis of single chirality SWNTs. To meet the demands of single chirality SWNTs with identical electrical and optical properties for potential applications, bulk synthesis of SWNTs with large quantity and low cost is necessary. So far, there are many SWNT products, such as CoMoCAT, HiPco, and TUBALL, that have been commercialized for industrial and research purposes. Particularly, the technology owed by OCSiAl company is notable for generating SWNTs in tonnes to enable low enough pricing for industrial applications to become economically feasible. However, the SWNTs have diverse structures and are not suitable for killer applications. Similarly, high-purity single chirality SWNT synthesis is realized on surface growth, while bulk growth of these SWNTs has not yet accomplished. (vii) To synthesize horizontally aligned SWNTs with high density. As reported by Zhang et al.<sup>[38]</sup> the density of

horizontally aligned SWNTs with almost single chirality is only 20 tubes  $\mu\text{m}^{-1}$ , which is much lower than the density demanded for SWNT-driven electronics (125 tubes  $\mu\text{m}^{-1}$ ).<sup>[17]</sup> In general, the high chirality selectivity is obtained at the expense of SWNT yield. Consequently, how to increase SWNT growth yield while maintaining the single chirality feature is one of the most challenging tasks in SWNT synthesis field. Therefore, further effort, like the “smart poisoning” of catalyst,<sup>[102]</sup> should be made to improve the SWNT selectivity without sacrificing the SWNT yield. (viii) Low-temperature growth of SWNTs. Horizontally aligned SWNTs with a high density are usually grown at temperatures above 900 °C. For present back-end CMOS technology, a maximum temperature of 400–450 °C is set by the mechanical integrity of low dielectric constant intermetal dielectrics. Surface-bound growth of SWNTs is achieved at 350 °C<sup>[154]</sup> and chirality-selective synthesis is also reported on silica-supported Ni catalyst at 450 °C.<sup>[96]</sup> Nevertheless, low-temperature synthesis of horizontally aligned SWNTs has not yet been attained. (ix) To deposit/grow horizontally aligned SWNTs onto any arbitrary substrates. Efficient growth of SWNTs are generally realized on substrates such as SiO<sub>2</sub>, MgO, and Al<sub>2</sub>O<sub>3</sub>. Other substrates, particular plastic ones, are unsuitable for acting as catalyst support for high-temperature SWNT synthesis. Alternatively, the deposition technique is suitable for transferring SWNTs onto any substrates by collecting SWNTs at the outlet of CVD reactor or dry transfer SWNTs from filters without using any solvent.<sup>[155]</sup> As the collection of SWNTs is at zones near room temperature, this approach sidesteps the high temperature required for synthesizing SWNTs. However, how to deposit parallel SWNTs onto arbitrary substrates is still insurmountable so far.

Based on Moore’s prediction,<sup>[156]</sup> a silicon-based device with desired dimensions for 2020 technologies will not be able to provide necessary performances any more. Although SWNTs have long been considered as an ideal replacement for silicon, there are still many obstacles that hinder their applications. Once the material hurdle is removed, nanotechnologies of the future in many areas will build on the advantages of identical SWNTs. However, these goals cannot be reached without the sustained efforts from carbon community. Continued efforts in carbon nanotube research and development fields are demanded in the future to fulfill the anticipated potential.

## Acknowledgements

The authors would also like to acknowledge the Ministry of Science and Technology of China (2016YFA0200101 and 2016YFA0200104), the National Natural Science Foundation of China (Grant Nos. 21233001, 21790052, and 51720105003), Taishan Scholars Program, the Natural Science Foundation of Shandong Province of China (Grant No. ZR2016EMM10), and Scientific Research Foundation of Shandong University of Science and Technology for Recruited Talents (Grant No. 2016RCJ001).

## Conflict of Interest

The authors declare no conflict of interest.

## Keywords

chirality-specific synthesis, growth kinetics, nucleation thermodynamics, single-walled carbon nanotubes, the tube–catalyst interface

Received: February 5, 2018

Revised: May 9, 2018

Published online: August 30, 2018

- [1] S. Iijima, *Nature* **1991**, 354, 56.
- [2] S. Iijima, T. Ichihashi, *Nature* **1993**, 363, 603.
- [3] D. S. Bethune, C. H. Kiang, M. S. de Vries, G. Gorman, R. Savoy, Z. Vazquez, R. Beryes, *Nature* **1993**, 363, 605.
- [4] N. Hamada, S. Sawada, A. Oshiyama, *Phys. Rev. Lett.* **1992**, 68, 1579.
- [5] J. W. Mintmire, B. I. Dunlap, C. T. White, *Phys. Rev. Lett.* **1992**, 68, 631.
- [6] C. T. White, J. W. Mintmire, *J. Phys. Chem. B* **2005**, 109, 52.
- [7] N. Wang, Z. K. Tang, G. D. Li, J. S. Chen, *Nature* **2000**, 408, 50.
- [8] M. He, J. Dong, K. Zhang, F. Ding, H. Jiang, A. Loiseau, J. Lehtonen, E. I. Kauppinen, *ACS Nano* **2014**, 8, 9657.
- [9] H. Kataura, Y. Kumazawa, Y. Maniwa, I. Urmez, S. Suzuki, Y. Ohtsuka, Y. Achiba, *Synth. Met.* **1999**, 103, 2555.
- [10] M. Ouyang, J. L. Huang, C. M. Lieber, *Acc. Chem. Res.* **2002**, 35, 1018.
- [11] A. D. Franklin, M. Luisier, S.-J. Han, G. Tulevski, C. M. Breslin, L. Gignac, M. S. Lundstrom, W. Haensch, *Nano Lett.* **2012**, 12, 758.
- [12] M. F. L. De Volder, S. H. Tawfik, R. H. Baughman, A. J. Hart, *Science* **2013**, 339, 535.
- [13] M. M. Shulaker, G. Hills, N. Patil, H. Wei, H. Y. Chen, H. S. Wong, S. Mitra, *Nature* **2013**, 501, 526.
- [14] M. S. Dresselhaus, G. Dresselhaus, R. Saito, A. Jorio, *Phys. Rep.* **2005**, 409, 47.
- [15] Z. Liu, Q. Zhang, L.-C. Qin, *Phys. Rev. B* **2005**, 71.
- [16] M. He, H. Jiang, E. I. Kauppinen, J. Lehtonen, *Nanoscale* **2012**, 4, 7394.
- [17] A. D. Franklin, *Nature* **2013**, 498, 443.
- [18] Z. Wu, Z. Chen, X. Du, J. M. Logan, J. Sippel, M. Nikolou, K. Kamaras, J. R. Reynolds, D. B. Tanner, A. F. Hebard, A. G. Rinzler, *Science* **2004**, 305, 1273.
- [19] M. Davenport, *Chem. Eng. News* **2015**, 93, 10.
- [20] S. Ghosh, S. M. Bachilo, R. B. Weisman, *Nat. Nanotechnol.* **2010**, 5, 443.
- [21] X. Tu, S. Manohar, A. Jagota, M. Zheng, *Nature* **2009**, 460, 250.
- [22] H. Liu, D. Nishide, T. Tanaka, H. Kataura, *Nat. Commun.* **2011**, 2, 309.
- [23] T. Lei, I. Pochorovski, Z. Bao, *Acc. Chem. Res.* **2017**, 50, 1096.
- [24] C. Luo, D. Wan, J. Jia, D. Li, C. Pan, L. Liao, *Nanoscale* **2016**, 8, 13017.
- [25] T. Guo, P. Nikolaev, A. Thess, D. T. Colbert, R. E. Smalley, *Chem. Phys. Lett.* **1995**, 243, 49.
- [26] M. José-Yacamán, M. Miki-Yoshida, L. Rendón, J. G. Santiesteban, *Appl. Phys. Lett.* **1993**, 62, 657.
- [27] Y. Li, W. Kim, Y. Zhang, M. Rolandi, A. Dunwei Wang, H. Dai, *J. Phys. Chem. B* **2001**, 105, 11424.
- [28] S. Reich, L. Li, J. Robertson, *Chem. Phys. Lett.* **2006**, 421, 469.
- [29] F. Ding, A. R. Harutyunyan, B. I. Yakobson, *Proc. Natl. Acad. Sci. USA* **2009**, 106, 2506.
- [30] A. R. Harutyunyan, G. Chen, T. M. Paronyan, E. M. Pigos, O. A. Kuznetsov, K. Hewaparakrama, S. M. Kim, D. Zakharov, E. A. Stach, G. U. Sumanasekera, *Science* **2009**, 326, 116.
- [31] S. M. Bachilo, L. Balzano, J. E. Herrera, F. Pompeo, D. E. Resasco, R. B. Weisman, *J. Am. Chem. Soc.* **2003**, 125, 11186.



- [32] S. Maruyama, Y. Miyauchi, Y. Murakami, S. Chiashi, *New J. Phys.* **2003**, *5*, 149.1.
- [33] X. Li, X. Tu, S. Zaric, K. Welscher, W. S. Seo, W. Zhao, H. Dai, *J. Am. Chem. Soc.* **2007**, *129*, 15770.
- [34] M. He, A. I. Chernov, P. V. Fedotov, E. D. Obraztsova, J. Sainio, E. Rikkinen, H. Jiang, Z. Zhu, Y. Tian, E. I. Kauppinen, M. Niemela, A. O. Krause, *J. Am. Chem. Soc.* **2010**, *132*, 13994.
- [35] H. Wang, Y. Yuan, L. Wei, K. Goh, D. Yu, Y. Chen, *Carbon* **2015**, *81*, 1.
- [36] F. Yang, X. Wang, D. Zhang, J. Yang, D. Luo, Z. Xu, J. Wei, J. Q. Wang, F. Peng, X. Li, R. Li, Y. Li, M. Li, X. Bai, F. Ding, *Nature* **2014**, *510*, 522.
- [37] J. R. Sanchez-Valencia, T. Dienel, O. Gröning, I. Shorubalko, A. Mueller, M. Jansen, K. Amsharov, P. Ruffieux, R. Fasel, *Nature* **2014**, *512*, 61.
- [38] S. Zhang, L. Kang, X. Wang, L. Tong, L. Yang, Z. Wang, K. Qi, S. Deng, Q. Li, X. Bai, F. Ding, J. Zhang, *Nature* **2017**, *543*, 234.
- [39] M. He, X. Duan, X. Wang, J. Zhang, Z. Liu, C. Robinson, *J. Phys. Chem. B* **2004**, *108*, 12665.
- [40] C. L. Cheung, A. Kurtz, H. Park, C. M. Lieber, *J. Phys. Chem. B* **2002**, *106*, 2429.
- [41] C. Feng, Y. Yao, J. Zhang, Z. Liu, *Nano Res.* **2009**, *2*, 768.
- [42] J. Xiao, S. Dunham, P. Liu, Y. Zhang, C. Kocabas, L. Moh, Y. Huang, K.-C. Hwang, C. Lu, W. Huang, *Nano Lett.* **2009**, *9*, 4311.
- [43] D. Yuan, L. Ding, H. Chu, Y. Feng, T. P. McNicholas, J. Liu, *Nano Lett.* **2008**, *8*, 2576.
- [44] S. Han, X. Liu, C. Zhou, *J. Am. Chem. Soc.* **2005**, *127*, 5294.
- [45] Y. Hu, L. Kang, Q. Zhao, H. Zhong, S. Zhang, L. Yang, Z. Wang, J. Lin, Q. Li, Z. Zhang, L. Peng, Z. Liu, J. Zhang, *Nat. Commun.* **2015**, *6*, 6099.
- [46] G. Hong, M. Zhou, R. Zhang, S. Hou, W. Choi, Y. S. Woo, J. Y. Choi, Z. Liu, J. Zhang, *Angew. Chem.* **2011**, *123*, 6804; *Angew. Chem., Int. Ed.* **2011**, *50*, 6819.
- [47] A. Ismach, L. Segev, E. Wachtel, E. Joselevich, *Angew. Chem.* **2004**, *116*, 6266; *Angew. Chem., Int. Ed.* **2004**, *43*, 6140.
- [48] M. Maret, B. Saubat, J. Flock, A. Mantoux, F. Charlot, D. Makarov, *Chem. Phys. Lett.* **2010**, *495*, 96.
- [49] L. Tang, Y. Luo, S. Zhang, Q. Zhang, Y. Yao, J. Zhang, *Carbon* **2018**, *126*, 313.
- [50] D. E. Resasco, W. E. Alvarez, F. Pompeo, L. Balzano, J. E. Herrera, B. Kitiyanan, A. Borgna, *J. Nanopart. Res.* **2002**, *4*, 131.
- [51] M. He, A. I. Chernov, P. V. Fedotov, E. D. Obraztsova, E. Rikkinen, Z. Zhu, J. Sainio, H. Jiang, A. G. Nasibulin, E. I. Kauppinen, M. Niemela, A. O. Krause, *Chem. Commun.* **2011**, *47*, 1219.
- [52] C. R. Henry, *Prog. Surf. Sci.* **2005**, *80*, 92.
- [53] M. He, H. Jiang, I. Kauppi, P. V. Fedotov, A. I. Chernov, E. D. Obraztsova, F. Cavalca, J. B. Wagner, T. W. Hansen, J. Sainio, E. Sairanen, J. Lehtonen, E. I. Kauppinen, *J. Mater. Chem. A* **2014**, *2*, 5883.
- [54] S. Huang, X. Cai, J. Liu, *J. Am. Chem. Soc.* **2003**, *125*, 5636.
- [55] S. Huang, M. Woodson, R. Smalley, J. Liu, *Nano Lett.* **2004**, *4*, 1025.
- [56] L. Zheng, M. O'connell, S. Doorn, X. Liao, Y. Zhao, E. Akhadov, M. Hoffbauer, B. Roop, Q. Jia, R. Dye, *Nat. Mater.* **2004**, *3*, 673.
- [57] R. Zhang, Y. Zhang, Q. Zhang, H. Xie, W. Qian, F. Wei, *ACS Nano* **2013**, *7*, 6156.
- [58] M. S. He, L. L. Zhang, H. Jiang, H. Yang, F. Fossard, H. Z. Cui, Z. P. Sun, J. B. Wagner, E. I. Kauppinen, A. Loiseau, *Carbon* **2016**, *107*, 865.
- [59] M. He, H. Jiang, B. Liu, P. V. Fedotov, A. I. Chernov, E. D. Obraztsova, F. Cavalca, J. B. Wagner, T. W. Hansen, I. V. Anoshkin, E. A. Obraztsova, A. V. Belkin, E. Sairanen, A. G. Nasibulin, J. Lehtonen, E. I. Kauppinen, *Sci. Rep.* **2013**, *3*, 1460.
- [60] M. He, T. Yang, D. Shang, B. Xin, A. I. Chernov, E. D. Obraztsova, J. Sainio, N. Wei, H. Cui, H. Jiang, *Chem. Eng. J.* **2018**, *341*, 344.
- [61] N. P. Joshi, D. E. Spearot, D. Bhat, *J. Nanosci. Nanotechnol.* **2010**, *10*, 5587.
- [62] Y. Magnin, A. Zappelli, H. Amara, F. Ducastelle, C. Bichara, *Phys. Rev. Lett.* **2015**, *115*, 205502.
- [63] A. Moiala, A. G. Nasibulin, E. I. Kauppinen, *J. Phys.: Condens. Matter* **2003**, *15*, S3011.
- [64] R. Rao, N. Pierce, D. Liptak, D. Hooper, G. Sargent, S. L. Semiatin, S. Curtarolo, A. R. Harutyunyan, B. Maruyama, *ACS Nano* **2013**, *7*, 1100.
- [65] R. Rao, K. G. Eyink, B. Maruyama, *Carbon* **2010**, *48*, 3971.
- [66] P. B. Balbuena, J. Zhao, S. Huang, Y. Wang, N. Sakulchaicharoen, D. E. Resasco, *J. Nanosci. Nanotechnol.* **2006**, *6*, 1247.
- [67] F. Abild-Pedersen, J. K. Nørskov, J. R. Rostrup-Nielsen, J. Sehested, S. Helveg, *Phys. Rev. B* **2006**, *73*, 115419.
- [68] A. Rinaldi, J. P. Tessonier, M. E. Schuster, R. Blume, F. Girgsdies, Q. Zhang, T. Jacob, S. B. Abd Hamid, D. S. Su, R. Schlögl, *Angew. Chem.* **2011**, *123*, 3373; *Angew. Chem., Int. Ed.* **2011**, *50*, 3313.
- [69] S. Helveg, C. Lopez-Cartes, J. Sehested, P. L. Hansen, B. S. Clausen, J. R. Rostrup-Nielsen, F. Abild-Pedersen, J. K. Nørskov, *Nature* **2004**, *427*, 426.
- [70] S. Hofmann, R. Sharma, C. Ducati, G. Du, C. Mattevi, C. Cepek, M. Cantoro, S. Pisana, A. Parvez, F. Cervantes-Sodi, A. C. Ferrari, R. Dunin-Borkowski, S. Lizzit, L. Petaccia, A. Goldoni, J. Robertson, *Nano Lett.* **2007**, *7*, 602.
- [71] M. Picher, P. A. Lin, J. L. Gomez-Ballesteros, P. B. Balbuena, R. Sharma, *Nano Lett.* **2014**, *14*, 6104.
- [72] H. Yoshida, T. Shimizu, T. Uchiyama, H. Kohno, Y. Homma, S. Takeda, *Nano Lett.* **2009**, *9*, 3810.
- [73] H. Yoshida, S. Takeda, T. Uchiyama, H. Kohno, Y. Homma, *Nano Lett.* **2008**, *8*, 2082.
- [74] M. He, H. Jin, L. Zhang, H. Jiang, T. Yang, H. Cui, F. Fossard, J. B. Wagner, M. Karppinen, E. I. Kauppinen, *Carbon* **2016**, *110*, 243.
- [75] B. Liu, D.-M. Tang, C. Sun, C. Liu, W. Ren, F. Li, W.-J. Yu, L.-C. Yin, L. Zhang, C. Jiang, *J. Am. Chem. Soc.* **2010**, *133*, 197.
- [76] B. Liu, W. Ren, L. Gao, S. Li, S. Pei, C. Liu, C. Jiang, H.-M. Cheng, *J. Am. Chem. Soc.* **2009**, *131*, 2082.
- [77] S. M. Huang, Q. R. Cai, J. Y. Chen, Y. Qian, L. J. Zhang, *J. Am. Chem. Soc.* **2009**, *131*, 2094.
- [78] S. Zhang, L. Tong, Y. Hu, L. Kang, J. Zhang, *J. Am. Chem. Soc.* **2015**, *137*, 8904.
- [79] M. He, H. Jiang, J. Lehtonen, E. I. Kauppinen, *Nanoscale* **2013**, *5*, 10200.
- [80] P. Li, X. Zhang, J. Liu, *Chem. Mater.* **2016**, *28*, 870.
- [81] D. A. Gomez-Gualdrón, G. D. McKenzie, J. F. J. Alvarado, P. B. Balbuena, *ACS Nano* **2012**, *6*, 720.
- [82] Y. Liu, A. Dobrinsky, B. I. Yakobson, *Phys. Rev. Lett.* **2010**, *105*, 235502.
- [83] V. I. Artyukhov, E. S. Penev, B. I. Yakobson, *Nat. Commun.* **2014**, *5*, 4892.
- [84] F. Cervantes-Sodi, T. P. McNicholas, J. G. Simmons, J. Liu, G. Csanyi, A. C. Ferrari, S. Curtarolo, *ACS Nano* **2010**, *4*, 6950.
- [85] L. An, J. M. Owens, L. E. McNeil, J. Liu, *J. Am. Chem. Soc.* **2002**, *124*, 13688.
- [86] M.-F. Fiawoo, A.-M. Bonnot, H. Amara, C. Bichara, J. Thibault-Pénisson, A. Loiseau, *Phys. Rev. Lett.* **2012**, *108*, 195503.
- [87] M. Diarra, A. Zappelli, H. Amara, F. Ducastelle, C. Bichara, *Phys. Rev. Lett.* **2012**, *109*, 185501.
- [88] M. He, Y. Magnin, H. Jiang, H. Amara, E. I. Kauppinen, A. Loiseau, C. Bichara, *Nanoscale* **2018**, *10*, 6744.
- [89] M. He, Y. Magnin, H. Amara, H. Jiang, H. Cui, F. Fossard, A. Castan, E. Kauppinen, A. Loiseau, C. Bichara, *Carbon* **2017**, *113*, 231.
- [90] S. Reich, L. Li, J. Robertson, *Phys. Rev. B* **2005**, *72*, 165423.

- [91] Y. Miyauchi, S. Chiashi, Y. Murakami, Y. Hayashida, S. Maruyama, *Chem. Phys. Lett.* **2004**, *387*, 198.
- [92] M. He, B. Liu, A. I. Chernov, E. D. Obraztsova, I. Kauppi, H. Jiang, I. Anoshkin, F. Cavalca, T. W. Hansen, J. B. Wagner, A. G. Nasibulin, E. I. Kauppinen, J. Linnekoski, M. Niemelä, J. Lehtonen, *Chem. Mater.* **2012**, *24*, 1796.
- [93] C. Zoican Loebick, R. Podila, J. Reppert, J. Chudow, F. Ren, G. L. Haller, A. M. Rao, L. D. Pfefferle, *J. Am. Chem. Soc.* **2010**, *132*, 11125.
- [94] B. Liu, W. Ren, S. Li, C. Liu, H. M. Cheng, *Chem. Commun.* **2012**, *48*, 2409.
- [95] Z. Ghorannevis, T. Kato, T. Kaneko, R. Hatakeyama, *J. Am. Chem. Soc.* **2010**, *132*, 9570.
- [96] M. He, A. I. Chernov, E. D. Obraztsova, J. Sainio, E. Rikkinen, H. Jiang, Z. Zhu, A. Kaskela, A. G. Nasibulin, E. I. Kauppinen, M. Niemelä, O. Krause, *Nano Res.* **2011**, *4*, 334.
- [97] M. He, P. V. Fedotov, A. Chernov, E. D. Obraztsova, H. Jiang, N. Wei, H. Cui, J. Sainio, W. Zhang, H. Jin, *Carbon* **2016**, *108*, 521.
- [98] K. Cui, A. Kumamoto, R. Xiang, H. An, B. Wang, T. Inoue, S. Chiashi, Y. Ikuhara, S. Maruyama, *Nanoscale* **2016**, *8*, 1608.
- [99] W.-H. Chiang, R. Mohan Sankaran, *Nat. Mater.* **2009**, *8*, 882.
- [100] Z. Zhu, H. Jiang, T. Susi, A. G. Nasibulin, E. I. Kauppinen, *J. Am. Chem. Soc.* **2011**, *133*, 1224.
- [101] H. Wang, B. Wang, X. Y. Quek, L. Wei, J. W. Zhao, L. J. Li, M. B. Chan-Park, Y. H. Yang, Y. A. Chen, *J. Am. Chem. Soc.* **2010**, *132*, 16747.
- [102] Y. Yuan, H. E. Karahan, C. Yildirim, L. Wei, Ö. Birer, S. Zhai, R. Lau, Y. Chen, *Nanoscale* **2016**, *8*, 17705.
- [103] F. Yang, X. Wang, D. Zhang, K. Qi, J. Yang, Z. Xu, M. Li, X. Zhao, X. Bai, Y. Li, *J. Am. Chem. Soc.* **2015**, *137*, 8688.
- [104] F. Yang, X. Wang, J. Si, X. Zhao, K. Qi, C. Jin, Z. Zhang, M. Li, D. Zhang, J. Yang, *ACS Nano* **2016**, *11*, 186.
- [105] E. S. Penev, V. I. Artyukhov, B. I. Yakobson, *ACS Nano* **2014**, *8*, 1899.
- [106] Q. Zhao, Z. Xu, Y. Hu, F. Ding, J. Zhang, *Sci. Adv.* **2016**, *2*, e1501729.
- [107] Z. Xu, T. Yan, F. Ding, *Chem. Sci.* **2018**, *9*, 3056.
- [108] G. Brinkmann, P. Fowler, D. Manolopoulos, A. Palsler, *Chem. Phys. Lett.* **1999**, *315*, 335.
- [109] H. Zhu, K. Suenaga, J. Wei, K. Wang, D. Wu, *J. Cryst. Growth* **2008**, *310*, 5473.
- [110] H. Zhu, K. Suenaga, A. Hashimoto, K. Urita, K. Hata, S. Iijima, *Small* **2005**, *1*, 1180.
- [111] S. Hofmann, G. Csanyi, A. Ferrari, M. Payne, J. Robertson, *Phys. Rev. Lett.* **2005**, *95*, 036101.
- [112] S. Nave, B. Jackson, *Phys. Rev. Lett.* **2007**, *98*, 173003.
- [113] Q. H. Yuan, H. Hu, F. Ding, *Phys. Rev. Lett.* **2011**, *107*, 156101.
- [114] D. C. Sorescu, D. L. Thompson, M. M. Hurley, C. F. Chabalowski, *Phys. Rev. B* **2002**, *66*, 035416.
- [115] R. Baker, M. Barber, P. Harris, F. Feates, R. Waite, *J. Catal.* **1972**, *26*, 51.
- [116] A. Kock, P. De Bokx, E. Boellaard, W. Klop, J. W. Geus, *J. Catal.* **1985**, *96*, 468.
- [117] J. Rostrup-Nielsen, D. L. Trimm, *J. Catal.* **1977**, *48*, 155.
- [118] I. Alstrup, *J. Catal.* **1988**, *109*, 241.
- [119] O. V. Yazyev, A. Pasquarello, *Phys. Rev. Lett.* **2008**, *100*, 156102.
- [120] F. Ding, P. Larsson, J. A. Larsson, R. Ahuja, H. Duan, A. Rosen, K. Bolton, *Nano Lett.* **2008**, *8*, 463.
- [121] W. Burton, N. Cabrera, F. Frank, *Nature* **1949**, *163*, 398.
- [122] Q. Yuan, F. Ding, *Angew. Chem.* **2015**, *127*, 6022; *Angew. Chem., Int. Ed.* **2015**, *54*, 5924.
- [123] H. Dumlich, S. Reich, *Phys. Rev. B* **2010**, *82*, 085421.
- [124] R. Rao, D. Liptak, T. Cherukuri, B. I. Yakobson, B. Maruyama, *Nat. Mater.* **2012**, *11*, 213.
- [125] V. I. Artyukhov, Y. Liu, B. I. Yakobson, *Proc. Natl. Acad. Sci. USA* **2012**, *109*, 15136.
- [126] S. M. Bachilo, M. S. Strano, C. Kittrell, R. H. Hauge, R. E. Smalley, R. B. Weisman, *Science* **2002**, *298*, 2361.
- [127] K. Hirahara, M. Kociak, S. Bandow, T. Nakahira, K. Itoh, Y. Saito, S. Iijima, *Phys. Rev. B* **2006**, *73*, 195420.
- [128] R. E. Smalley, Y. B. Li, V. C. Moore, B. K. Price, R. Colorado, H. K. Schmidt, R. H. Hauge, A. R. Barron, J. M. Tour, *J. Am. Chem. Soc.* **2006**, *128*, 15824.
- [129] Z. Ren, *Nat. Nanotechnol.* **2007**, *2*, 17.
- [130] Y. Yao, C. Feng, J. Zhang, Z. Liu, *Nano Lett.* **2009**, *9*, 1673.
- [131] J. Liu, C. Wang, X. Tu, B. Liu, L. Chen, M. Zheng, C. Zhou, *Nat. Commun.* **2012**, *3*, 1199.
- [132] B. Liu, J. Liu, X. Tu, J. Zhang, M. Zheng, C. Zhou, *Nano Lett.* **2013**, *13*, 4416.
- [133] X. Yu, J. Zhang, W. Choi, J.-Y. Choi, J. M. Kim, L. Gan, Z. Liu, *Nano Lett.* **2010**, *10*, 3343.
- [134] H. Omachi, T. Nakayama, E. Takahashi, Y. Segawa, K. Itami, *Nat. Chem.* **2013**, *5*, 572.
- [135] D. Dutta, W.-H. Chiang, R. M. Sankaran, V. R. Bhethanabotla, *Carbon* **2012**, *50*, 3766.
- [136] W. E. Alvarez, B. Kitiyanan, A. Borgna, D. E. Resasco, *Carbon* **2001**, *39*, 547.
- [137] G. Lolli, L. Zhang, L. Balzano, N. Sakulchaicharoen, Y. Tan, D. E. Resasco, *J. Phys. Chem. B* **2006**, *110*, 2108.
- [138] A. Jorio, A. Santos, H. Ribeiro, C. Fantini, M. Souza, J. Vieira, C. Furtado, J. Jiang, R. Saito, L. Balzano, D. Resasco, M. Pimenta, *Phys. Rev. B* **2005**, *72*, 075207.
- [139] M. He, A. I. Chernov, E. D. Obraztsova, H. Jiang, E. I. Kauppinen, J. Lehtonen, *Carbon* **2013**, *52*, 590.
- [140] N. Li, X. Wang, F. Ren, G. L. Haller, L. D. Pfefferle, *J. Phys. Chem. C* **2009**, *113*, 10070.
- [141] M. Fouquet, B. C. Bayer, S. Esconjauregui, R. Blume, J. H. Warner, S. Hofmann, R. Schlogl, C. Thomsen, J. Robertson, *Phys. Rev. B* **2012**, *85*, 235411.
- [142] M. He, X. Wang, L. Zhang, Q. Wu, X. Song, A. I. Chernov, P. V. Fedotov, E. D. Obraztsova, J. Sainio, H. Jiang, *Carbon* **2018**, *128*, 249.
- [143] M. S. He, P. V. Fedotov, E. D. Obraztsova, V. Viitanen, J. Sainio, H. Jiang, E. I. Kauppinen, M. Niemela, J. Lehtonen, *Carbon* **2012**, *50*, 4294.
- [144] B. Wang, L. Wei, L. Yao, L. J. Li, Y. Yang, Y. Chen, *J. Phys. Chem. C* **2007**, *111*, 14612.
- [145] S. Lim, C. Wang, Y. Yang, D. Ciuparu, L. Pfefferle, G. L. Haller, *Catal. Today* **2007**, *123*, 122.
- [146] H. Wang, L. Wei, F. Ren, Q. Wang, L. D. Pfefferle, G. L. Haller, Y. Chen, *ACS Nano* **2012**, *7*, 614.
- [147] Y. Yuan, L. Wei, W. C. Jiang, K. Goh, R. R. Jiang, R. Lau, Y. Chen, *J. Mater. Chem. A* **2015**, *3*, 3310.
- [148] A. S. Anisimov, A. G. Nasibulin, H. Jiang, P. Launois, J. Cambedouzou, S. D. Shandakov, E. I. Kauppinen, *Carbon* **2010**, *48*, 380.
- [149] S. Mazzucco, Y. Wang, M. Tanase, M. Picher, K. Li, Z. J. Wu, S. Irle, R. Sharma, *J. Catal.* **2014**, *319*, 54.
- [150] M. Lin, J. P. Ying Tan, C. Boothroyd, K. P. Loh, E. S. Tok, Y. L. Foo, *Nano Lett.* **2006**, *6*, 449.
- [151] L. Zhang, M. He, T. W. Hansen, J. Kling, H. Jiang, E. I. Kauppinen, A. Loiseau, J. B. Wagner, *ACS Nano* **2017**, *11*, 4483.
- [152] J. Wang, P. Liu, B. Xia, H. Wei, Y. Wei, Y. Wu, K. Liu, L. Zhang, Q. Li, S. Fan, K. Jiang, *Nano Lett.* **2016**, *16*, 4102.
- [153] R. Fasel, P. Ruffieux, J. R. S. Valencia, M. Jansen, A. Müller, K. Amsharov, *Google Patents EP2933228A1*, **2017**.
- [154] M. Cantoro, S. Hofmann, S. Pisana, V. Scardaci, A. Parvez, C. Ducati, A. C. Ferrari, A. M. Blackburn, K.-Y. Wang, J. Robertson, *Nano Lett.* **2006**, *6*, 1107.
- [155] A. G. Nasibulin, A. Kaskela, K. Mustonen, A. S. Anisimov, V. Ruiz, S. Kivisto, S. Rackauskas, M. Y. Timmermans, M. Pudas, B. Aitchison, *ACS Nano* **2011**, *5*, 3214.
- [156] G. E. Moore, *Proc. IEEE* **1998**, *86*, 82.